# Measurement and model analyses of the ozone variation during 2006 to 2015 and its response to emission change in megacity Shanghai, China

Jianming Xu[1,2], Xuexi Tie[3,4], Wei Gao[1,2], Yanfen Lin[5], and Qingyan Fu[5]

[1] Yangtze River Delta Center for Environmental Meteorology Prediction and Warning, Shanghai Meteorological Service, Shanghai, 200135, China
[2] Shanghai Key Laboratory of Health and Meteorology, Shanghai Meteorological Service, Shanghai, 200135, China
[3] Key Laboratory of Aerosol Chemistry & Physics, SKLLQG, Institute of Earth Environment, Chinese Academy of Science, Xi'an, 710061, China
[4] Center for Excellence in Urban Atmospheric Environment, Institute of Urban Environment, Chinese Academy of Science, Xiamen, 361021, China
[5] Shanghai Environmental Monitoring Center, Shanghai, 200135, China

Correspondence: Xuexi Tie (tiexx@ieecas.cn)

**Abstract.** The fine particles ($PM_{2.5}$) in China decrease significantly in recent years as a result of the implement of Chinese Clean Air Action Plan since 2013, while the $O_3$ pollution is getting worse, especially in megacities such as Beijing and Shanghai. Better understanding the elevated $O_3$ pollution in Chinese megacities and its response to emission change is important for developing an effective emission control strategy in future. In this study, we analyze the significant increasing trend of daily maximum $O_3$ concentration from 2006 to 2015 in the megacity Shanghai with the variability of 0.8-1.3 ppbv $yr^{-1}$. It is likely attributed to the notable reduction of $NO_x$ concentration with the decreasing rate of 1.86-2.15 ppbv $yr^{-1}$ accompanied with the little change of VOCs during the same period by excluding the weak trends of meteorological impacts on local dispersion (wind speed), regional transport (wind direction) and $O_3$ photolysis (solar radiation). It is further illustrated by using a state of the art regional chemical/dynamical model (WRF-Chem) to explore the $O_3$ variation response to the reduction of $NO_x$ emission in Shanghai. The control experiment conducted for September of 2009 shows very excellent performance for $O_3$ and $NO_x$ simulations including both the spatial distribution pattern, and the day by day variation through comparing with 6 in-situ measurements from MIRAGE-shanghai field campaign. Sensitive experiments with 30% reduction of $NO_x$ emission from 2009 to 2015 in Shanghai estimated by Shanghai Environmental Monitoring Center shows that the calculated $O_3$ concentrations exhibit obvious enhancement by 4-7 ppbv in urban zones with the increasing variability of 0.96-1.06 ppbv $yr^{-1}$, which is well consistent with the observed $O_3$ trend as a result of the strong VOC-limited condition for $O_3$ production. The large reduction of $NO_x$ combined with less change of VOCs during the past ten years promotes the $O_3$ production in Shanghai to move towards $NO_x$-limited regime. Further analysis of WRF-Chem experiments and $O_3$ isopleths diagram suggests that the $O_3$ production in downtown is still under VOC-limited regime after 2015 despite of the remarkable $NO_x$ reduction, while moves to the transition regime between $NO_x$-limited and VOC-limited in sub-urban zones. Supposing the insignificant VOCs variation persists, the $O_3$ concentration in downtown would keep increasing till 2020 with the further 20% reduction of $NO_x$ emission after 2015 estimated by Shanghai Clean Air Action Plan. The $O_3$ production in Shanghai will switch from VOC-limited to $NO_x$-limited regime after 2020 except downtown area which is likely close to the transition regime. As a result the $O_3$ concentration will decrease by 2-3 ppbv in sub-urban zones, and more than 4 ppbv in suburb response to 20% reduction of $NO_x$ emission after 2020, whereas is not sensitive to both $NO_x$ and VOCs changes in downtown. This result reveals that the control strategy of $O_3$ pollution is a very complex process, and needs to be carefully studied.

**Key Words: $O_3$ pollution in Shanghai, Long-term O3 trend, WRF-Chem**

## 1 Introduction

Ozone ($O_3$) in the troposphere plays the important role in the oxidation of chemically and climatically relevant trace gases, hence regulating their lifetime in the atmosphere (Monks et al., 2015). In the lower troposphere, $O_3$ is produced from photochemical reactions involving volatile organic compounds (VOCs, broadly including CO) and nitrogen oxides ($NO_x$ = NO + $NO_2$) in the presence of sunlight (Brasseur et al., 1999). As a strong oxidant, $O_3$ at ground level is detrimental to human health and vegetation (Tai et al., 2014), and has been received continuous attention from both the scientific and regulatory communities in the past three decades.

Shanghai has emerged as one of the largest megacities in the world over the last two decades. The city has a fleet of over 3.6 million vehicles and the population of over 2400 million permanent residents, which results in high emissions of $NO_x$, VOCs, and primary particulate matter (PM) to the atmosphere from industrial and commercial activities, leading to the photochemical smog formation. Persistent high level of surface $O_3$ and PM were observed in Shanghai during the past ten years (Geng et al., 2007; Ran et al., 2009; Tie et al., 2009a; Xu et al., 2015). In order to mitigate the adverse impacts from severe air pollution, the Clean Air Action Plan was issued in the end of 2013 to implement the emission reduction program in Shanghai and its neighboring area. As a result, the annual mean $PM_{2.5}$ (particles with diameter $\leqq$ 2.5 μm) mass concentration has decreased from 50 μg $m^{-3}$ in 2013 to 39 μg $m^{-3}$ in 2017. However $O_3$ pollution has been continuously worsen, with the non-attainment days (daily maximum $O_3$ concentration exceeding 200 μg $m^{-3}$, or daily maximum 8h-$O_3$ concentration exceeding 100 μg $m^{-3}$) increased from 99 d in 2014 to 129 d in 2016. As a result, $O_3$ has became the primary air pollutant affecting the ambient air quality instead of $PM_{2.5}$ in Shanghai. Similar issue has also been occurred in other cities in the eastern China (Lu et al., 2018). For example, the mean $PM_{2.5}$ mass concentration over the 74 major cites decreased by 40% from 2013 to 2017, whereas the maximum daily 8-h average $O_3$ concentration in summer exceeds the Chinese National Ambient Air Quality Stand (GB3095-2012) over most of eastern China (Li et al., 2019). Thus better understanding the causes of elevated $O_3$ in China is important for developing effective $O_3$ control strategies, especially in megacities such as Shanghai.

A prerequisite to an effective emission-based $O_3$ control strategy is to understand the temporal and spatial relationship between $O_3$ and its precursors, and the response of $O_3$ concentrations to the changes in emissions of $O_3$-precursors (such as $NO_x$ and VOCs, Lin et al., 1988). The relationship of $O_3$ and $O_3$-precursors can be clarified as $NO_x$-limited or VOC-limited chemistry of $O_3$ formation, which is usually defined based on the relative impact of a given percent reduction in $NO_x$ relative to VOCs in the context of urban chemistry (Sillman, 1999).

Some observational and modeling works on $O_3$ chemical formation and transformation have been carried out in Shanghai since 2007. The $O_3$ production in Shanghai city is clearly under VOC-limited regime (Geng et al., 2007), in which the aromatics and alkenes play the dominant roles (Geng et al., 2008a). The aircraft measurements in Yangtze River Delta (YRD) region show the strong anti-correlation between $NO_x$ and $O_3$ during noontime, indicating the similar VOC-limited regime for $O_3$ production in the area neighboring Shanghai (Geng et al., 2008b). Thus either $NO_x$ reduction or VOCs growth is favorable for $O_3$ enhancement in Shanghai. Gao et al. (2017) reported that $O_3$ concentration in Shanghai downtown increased 67% from 2006 to 2015, whereas $NO_x$ concentration decreased about 38%. This is also consistent with the results of Lin et al. (2017) that, the median of the maximum daily 8-h average $O_3$ concentration in Shanghai

increased notably from 2006 to 2016, with the rate of 1.4 ppbv $yr^{-1}$, while the $NO_2$ decreased from 66.7 to 42.1 $\mu g\ m^{-3}$ with about 20% reduction. These previous studies provide the useful information regarding the $O_3$ chemical formation and transformation in Shanghai. However, such $O_3$ variation responding to emission change has not been clearly investigated. Considering that $O_3$ formation is a complicated process including chemistry, transport, emission, deposition and their interactions, the chemical transport model is the powerful tool to gain an understanding of these interacting processes. For example, Lei et al. (2007), Ying et al. (2009) and Song et al. (2010) investigated the $O_3$ production rate and its sensitivity to emission changes of $O_3$ precursors by CAMx model in Mexico City Metropolitan Area (MCMA). Tie et al. (2013) analyzed the comprehensive data of the MIRAGE-Shanghai field campaign by WRF-Chem model, and quantified the threshold value by the emission ratio of $NO_x$/VOCs for switching from VOC-limited to $NO_x$-limited in Shanghai. Recently Li et al. (2019) suggested an important cause of the increasing $O_3$ in North China Plain (NCP) during 2013 to 2017 as the significant decrease in $PM_{2.5}$ slowing down the sink of hydroperoxy radicals and thus speeding up the $O_3$ production by GOES-CHEM model. However such implication for $O_3$ trend is not pervasive in YRD and other regions. Moreover, the 5-year $O_3$ records seem rather short to examine the inter-annual variability of $O_3$ concentration. The GOES-CHEM experiment with 50 km resolution maybe is suitable for the $O_3$ simulation at regional scale but is too coarse to resolve the local $O_3$ budget at urban scale, such as Beijing or Shanghai. To our knowledge, there are no peer-reviewed modeling studies focus on the past long term $O_3$ variations response to emission changes conducted in Shanghai. Thus this paper extends the study of Tie et al. (2013) and Gao et al. (2017) to not only further examine the inter-annual $O_3$ variations from a larger scale with more comprehensive measurements, but also explore the $O_3$ enhancement response to $NO_x$ reduction in Shanghai and predict the future $O_3$ variations by models. The effects of emission changes on long term $O_3$ variability are evaluated by WRF-Chem model with high resolution and compared with measurements. The shift of $O_3$ photochemical regime relative to the variations of $NO_x$ and VOCs concentrations in the past ten years is discussed by $O_3$ isopleths diagram combined with WRF-Chem model to provide more insights into the $O_3$ control strategy. Moreover, the future $O_3$ levels and its possible chemical regime in Shanghai are also discussed according to the Shanghai Clean Air Action Plan.

The paper is constructed as follows. The measurements and models used for this study are described in Sect. 2. The analysis on the long-term in-situ measurements of $O_3$ and its precursors, as well as the model sensitive experiments are presented and discussed in Sect. 3-6. The conclusion is summarized in Sect. 7.

## 2 Measurements and models

### 2.1 Measurements

The measurements of $O_3$ and $NO_x$ are collected from 6 sites (XJH, PD, JS, BS, SS, DT) over Shanghai (Fig. 1 a) under different influence of air pollutant emissions. The XJH site is located at the downtown of Shanghai, which is strongly influenced by emission of transportation. The PD site is located at the sub-urban area near a big park, which is influenced by the mixed emissions of transportation and residential. The JS site is located in the south of Shanghai with several large chemical industries. The BS site is located in the north of Shanghai with some big steel and power

plants. The SS site is located at the top of a sole hill (100 m a.g.l) in Shanghai, which has minor effect from local emissions, and is influenced by regional transport. The DT site is located at a remote island without anthropogenic activities. These $O_3$ and $NO_x$ measurements are used for the evaluation on WRF-Chem performance. In addition, the VOCs are sampled at the downtown site XJH and the sub-urban site PD, and are analyzed at a chemistry laboratory. The study on the $O_3$ chemical production in this paper is limited at XJH and PD by the intensive measurements of $O_3$ and its precursors (VOCs and $NO_x$) from 2006 to 2015. The meteorological measurements including wind speed and direction, solar radiation and temperature are collected at BS site, which is the only climatology observatory in Shanghai. The meteorological measurements in BS are used for international exchange of meteorological data representing Shanghai, sponsored by the World Meteorological Organization (WMO).

**2.2 Instruments**

$O_3$ is measured using an EC 9810 Ozone Analyzer, together with a UV photometer, which accurately and reliably measures $O_3$ concentration in ambient air. The oxides of nitrogen analyzer (EC9841B/ECOTECH) have a heated molybdenum $NO_2$ to NO converter. The resulting NO concentration is quantified using the chemiluminescence technique. This instrument is automated to set to be zero, and include an optional external valve manifold and external calibration sources. Quality control checks are performed every 3 days, including inspection of the shelter and instruments as well as zero, precision and span checks. Filter is replaced once every two weeks and calibration is made every month. The $O_3$ concentrations are recorded every 1 min.

VOCs concentrations are sampled for 24 h every day with a 6 L silonite canister with a silonite coated valve (model 29-10622). The internal silonite coating improves long-term VOC storage. The instrument has a large volume to detect volatile chemicals down to low pptv range. Absorption is eliminated by using nupropackless valves and by eliminating teflon tape in the valve stem. These canisters are recognized to meet or exceed the technical specifications required for EP methods TO14-A and TO15. Gases samples are pre-processed using Model 7100 VOC preconcentrator. Samples are analyzed for VOCs using a gas chromatography system (Agilent GC6890) coupled with mass-selective detection (Agilent MSD5975 N) with length of 60 m, diameter of 0.32 mm, and film thickness of 1.0 um. This measurement system can detect VOCs concentrations down to low pptv range.

These instruments to measure $O_3$, $NO_x$ and VOCs concentrations are calibrated carefully. Detail information for the instruments and the procedures to perform data quality control are described by Geng et al. (2007), Ran et al. (2009), Tie et al. (2013) and Gao et al. (2017). These data have been widely used to investigate the diurnal, seasonal and inter-annual variations of $O_3$ in Shanghai (Geng et al., 2007; 2015; Tang et al., 2008; Ran et al., 2009; Gao et al., 2017) and its chemical mechanism (Geng et al., 2008a; 2008b; Tie et al., 2009a; 2013).

**2.3 WRF-Chem model**

The regional chemical/transport model (Weather Research and Forecasting Chemical model-WRF-Chem) (Grell et al., 2005) is used to investigate the $O_3$ variations response to emission changes in Shanghai. The version of the model is improved mainly by Tie et al. (2007) and Li et al. (2010; 2011). The chemical mechanism chosen in WRF-Chem is the RADM2 (Regional Acid

Deposition Model, version 2) gas-phase chemical mechanism (Stockwell et al., 1990), which includes 158 reactions among 36 species. The fast radiation transfer module (FTUV) is developed and used to calculate photolysis rates (Tie et al., 2003), considering the impacts of aerosols and clouds on the photochemistry (Li et al., 2011). The aerosol modules are developed by EPA CMAQ (version 4.6) (Binkowski and Roselle, 2003). The wet deposition of chemical species is calculated by using the method in the CMAQ module and the dry deposition parameterization follows Wesely et al. (1989). The ISORROPIA version 1.7 is used to calculate the inorganic aerosols (Nenes et al., 1998). The secondary organic aerosol (SOA) is predicted using a non-traditional SOA module, including the volatility basis set (VBS) modeling approach in which primary organic components are assumed to be semi-volatile and photochemically reactive and are distributed in logarithmically spaced volatility bins. The partitioning of semi-volatile organic species is calculated supposing the bulk gas and particle phases are in equilibrium and all condensable organics form a pseudoideal solution. Nine surrogate species with saturation concentrations from $10^{-2}$ to $10^{6}$ μg $m^{-3}$ at room temperature are used for the primary organic aerosol (POA) components. The SOA contributions from glyoxal and methylglyoxal is also included. The major physical processes employed in WRF are summarized as the Lin microphysics scheme (Lin et al., 1983), the Yonsei University (YSU) PBL scheme (Hong et al., 2006), the Noah Land surface model (Chen and Dudhia, 2001), and the long wave radiation parameterization (Dudhia, 1989).

The domain is set up to cover a region (centered at 32.5°N, 118°E) of 356×345 grids with a horizontal resolution of 6 km (Zhou et al., 2017). The initial and lateral boundary conditions of the meteorology are extracted from the NCEP FNL reanalysis data. The lateral meteorological boundary is updated every 6 h. The chemical lateral boundary conditions are constrained by the global chemical transport model (MOART–Model for Ozone and Related chemical Tracers) with aerosol formation modules (Tie et al., 2001; Emmonset al., 2010). Both the chemical and dynamical integration step is set to be 60 s. The Multi-resolution Emission Inventory for China (MEIC) developed by Zhang et al. (2009) is used in WRF-Chem for the domain except Shanghai with $0.25^{o}$ resolution. The anthropogenic emissions (including CO, $NO_x$, $SO_2$ and VOCs) for Shanghai are developed by Tie et al. (2013) with $0.16^{o}$ resolution based on the MIRAGE-shanghai field campaign. $NO_x$ and $SO_2$ emissions in YRD region are adjusted by Zhou et al. (2017) according to the evaluation of WRF-Chem prediction for about 195 cities during 2014-2015. The distribution of $NO_x$ emission in 2009 in Shanghai is depicted in Fig. 1b. The biogenic emissions are calculated online using the MEGAN (Model of Emissions of Gases and Aerosol from Nature) model developed by Guenther et al. (2006).

**Figure 1.** (a) The distribution of land-use category in Shanghai. The blue dots denote the locations of 6 sties (XJH, BS, PD, SS, JS, DT). (b) The $NO_x$ emission of 2009 scenario in Shanghai.

### 2.4 OZIPR model

The ozone isopleths diagram for Shanghai is plot by OZIPR (Ozone Isopleths Plotting Package Research) model (Gery and Crouse, 2002). The OZIPR model employs a trajectory-based air quality simulation model in conjunction with the Empirical Kinetics Modeling Approach (EKMA) to relate $O_3$ concentrations levels of organic and nitrogen oxide emissions. OZIPR simulates complex chemical and physical processes of the lower atmosphere through a trajectory model. The physical representation is a well-mixed column of air extending from the ground to the top of

the mixed layer. Emissions from the surface are included as the air column passes over different emission sources, and air from above the column is mixed in as the inversion rises during the day. $O_3$ precursor concentrations and ambient information such as temperature, relative humidity and boundary layer height from measurements in Shanghai are specified for each single run. Therefore a series of simulations are performed to calculate peak $O_3$ concentration as a function of initial precursor concentrations (Tang et al., 2008; Geng et al., 2008b).

## 3 Variability of $O_3$ and its precursors measured in Shanghai

### 3.1Variation of $O_3$ concentration

Fig. 2a and b show the annual variation of daily maximum $O_3$ concentration at downtown site XJH and sub-urban site PD respectively from 2006 to 2015. The daily maximum $O_3$ concentrations increase notably during the past ten years with the increasing rate of 0.808 ppbv $yr^{-1}$ at XJH and 1.374 ppbv $yr^{-1}$ at PD respectively. In similar the daily maximum 8h-$O_3$ concentration also increased at the rate of 1.06 and 1.4 ppbv $yr^{-1}$ at XJH and PD respectively. It is consistent with the reported $O_3$ increasing trend ranging from 1-2 ppbv $yr^{-1}$ at background and urban sites in eastern China during 2001 to 2015 (Tang et al., 2009; Ma et al., 2016; Sun et al., 2016). In 2006, the mean daily maximum $O_3$ concentrations at XJH and PD are 25.2 ppbv and 32.7 ppbv respectively. While in 2017, the mean daily maximum $O_3$ concentrations at the two sites increase to 41.3 ppbv and 51.8 ppbv respectively, with 64% and 58% enhancement compared with that in 2006. The mean daily maximum $O_3$ concentration at downtown site XJH during 2006 to 2015 is 39.2 ppbv, which is significantly lower than that at sub-urban site PD of 50.7 ppbv, suggesting the $O_3$ is depressed in downtown area. Geng et al. (2007) suggested that the $O_3$ production in the city of Shanghai was under VOC-limited regime, thus higher $NO_x$ in downtown resulted in lower $O_3$ concentration. Considering the inhomogeneous spatial distribution of the precursors of $O_3$ in Shanghai (Geng et al. 2008a), we extend the analysis on inter-annual $O_3$ variations to a broader scope by using the $O_3$ measurements from 31 sites provided by Shanghai Environmental Monitoring Center, covering the entire Shanghai area. It is shown in Fig. 2c that the median of the $O_3$-8h concentration also increases significantly from 2006 to 2015, with the increasing rate of 1.571 ppbv $yr^{-1}$, indicating that the significant increasing trend of $O_3$ concentration not only occurs in the city of Shanghai, but also expanded to a larger area nearby Shanghai. Li et al. (2019) also reported a regional $O_3$ increasing phenomena in summer during 2013 to 2017 from Shanghai to Beijing in eastern China.

In order to analyze the individual contribution to the long-term $O_3$ trend, the variations of $O_3$ precursors, and meteorological parameters are measured and showed in the following sections.

**Figure 2.** The annual variation of daily maximum $O_3$ concentration (ppbv) from 2006 to 2015 at (a) downtown site XJH and (b) sub-urban site PD, both presenting the significant increasing trends with 0.808 ppbv $yr^{-1}$ at XJH and 1.374 ppbv $yr^{-1}$ at PD respectively. The variation of the median 8-h $O_3$ concentration (ppbv) from 2006 to 2015 averaged for 31 sites over Shanghai (c), also shows the increasing variability of 1.571 ppbv $yr^{-1}$.

### 3.2 Variations of the precursors ($NO_x$ and VOCs)

It is well known that the tropospheric $O_3$ formation is throughout a complicated photochemical process, and is strongly related to the precursors of $O_3$ (VOCs and $NO_x$). According to the previous

studies (Geng et al., 2007; Ran et al., 2009), the chemical formation of $O_3$ in Shanghai is revealed to be under VOC-limited. Thus either enhancement of VOCs or reduction in $NO_x$ would both result in the growth of $O_3$ concentration. In order to better understanding the factors possibly driving the $O_3$ increasing trend depicted in Fig. 2, the variations of $NO_x$ and VOCs concentrations at XJH and PD in the same period are presented in Fig. 3. The $NO_x$ concentrations present significant decreasing trend from 2006 to 2015 at both XJH and PD sites, which is opposite to the increasing trend of $O_3$ variations in Fig. 2. At XJH, the decreasing rate of $NO_x$ is 2.15 ppbv $yr^{-1}$, which is more remarkable than that at PD site of 1.86 ppbv $yr^{-1}$. According to the studies by Lin et al (2017), the reduction of $NO_x$ concentration in Shanghai was likely attributed to the implementation of stringent emission control strategy for transportation, including improvement of gas quality, popular usage of electricity cars, and limitation of heavy cars into the urban zones. These regulations significantly decrease the emissions of $NO_x$ into the atmosphere, resulting in lower $NO_x$ concentrations. Zheng et al. (2018) also reported the 30% reduction of $NO_x$ emission in the past 5 years in YRD region. In comparison, the VOCs concentrations at XJH and PD decrease very slightly during 2006 to 2015. At XJH, the mean VOCs concentration during 2013 to 2015 is about 20 ppbv, which is some lower than that during 2009 to 2012 (23 ppbv). At PD, the VOCs concentration shows strong inter-annual variations, ranging from 16 to 22 ppbv. Generally the VOCs concentration at the downtown site XJH is higher than that at the sub-urban site PD by 14%. It is consistent with the studies of Cai et al. (2010), suggesting that about 25% of VOCs is attributed to the vehicles in shanghai urban zones.

**Figure 3.** The mean annual concentrations (ppbv) of $NO_x$ (dots) and VOCs (bars) from 2006 to 2015 at (a) downtown site XJH and (b) sub-urban site PD respectively. The $NO_x$ concentrations at XJH and PD both present obvious decreasing trends with -2.1 ppbv $yr^{-1}$ and -1.87 ppbv $yr^{-1}$. While the VOCs concentrations at both sites present no clear inter-annual trends.

### 3.3 Meteorological impacts on $O_3$ photolysis, dispersion and transport

In addition to the precursors, meteorology such as solar radiation and wind speed and directions also plays the important roles in $O_3$ concentration through the photochemical and physical processes. Fig. 4 shows the annual variation of wind speed and total solar radiation from 2006 to 2015. The solar radiation presents weak annual variations ranging from 140 to 150 $Wm^{-2}$, exhibiting a large variability but without a significant trend. As a result, the variation of solar radiation cannot explain the significant change of $O_3$ concentration on the view of photolysis. The wind speed is usually regarded as the indicator for the dispersion capacity for air pollutants. Several studies reported that the wind speed in winter in eastern China presented decreasing variability during the past 40 years due to the decadal variation of winter monsoon affecting the haze occurrence (Wang et al., 2016; Zhao et al., 2016; Xu et al., 2017). While high $O_3$ events usually occur in summer season for middle-latitude cities such as Shanghai (Wang et al., 2017). The mean summer wind speed in Fig. 4a fluctuates between 3.3 $ms^{-1}$ to 3.9 $ms^{-1}$ during 2006 to 2015 except the minimum value in 2014 (2.9 $ms^{-1}$) due to fewer typhoon in the period. Without 2014, the variability of summer wind speed is insignificant, with a trend of -0.02 m $s^{-1}$ $yr^{-1}$, which could not be regarded as the dominant factor to interpret the increasing $O_3$ trend. Local $O_3$ concentration would be affected by transport of upstream plumes usually determined by wind

direction. Geng et al. (2011) suggested that $O_3$ concentration was higher in west wind compared with other wind sectors in Shanghai indicating the possible $O_3$ transport from western area out of Shanghai. Fig. 5 presents the annual wind rose at Baoshan site from 2006 to 2015, presenting the very similar pattern of wind direction in each year. The mean wind direction concentrates in the sector between 60-80 degree, suggesting the dominant wind in Shanghai is easterly accounting for 50%. The east wind in Shanghai usually carries with the clean air mass from the sea to improve the local air quality (Xu et al., 2015). The frequency of west wind changes little during 2006 and 2015 ranging from 10-15%, suggesting that the regional transport is not a major factor driving the $O_3$ increasing. Based on the above analysis, it is speculated that the rapid $O_3$ increasing during 2006–2015 in shanghai is likely attributed to the reduction of $NO_x$ concentration as a result of the VOC-limited condition for $O_3$ production.

**Figure 4.** The annual variation of (a) summer wind speed (m $s^{-1}$) and (b) total solar radiation (W $m^{-2}$) from 2006 to 2015 in Shanghai. Both wind speed and the solar radiation present weak inter-annual variations but without significant trends.

**Figure 5.** The wind rose in each year from 2006 to 2015 in Shanghai. The red line means the resultant vector suggesting the dominant wind direction.

### 3.4 Different $O_3$ variability in nighttime and daytime

The mean diurnal variations of $O_3$ concentrations between 2006 and 2015 are compared in Fig. 6a at XJH and PD sites respectively. The maximum and minimum $O_3$ concentrations occur in the afternoon (14-15 pm) and early morning (6-7 am) respectively at both sites. In addition, the diurnal $O_3$ concentrations at XJH and PD sites all increase significantly from 2006 to 2015. For example, the peak $O_3$ concentration at XJH increases from 21 ppbv to 37 ppbv, meanwhile the minimum $O_3$ concentration rises from 5 ppbv to 14 ppbv, exhibiting higher increasing rate. Similar diurnal $O_3$ enhancement is also observed at PD site during the same period. The $O_3$ chemical mechanism in daytime includes both production and loss processes. In contrast, in nighttime, the photochemical production ceases, and there mainly exists loss process for $O_3$. In addition both dry deposition and nighttime turbulence also have the influence in the nighttime $O_3$ concentration suggested by Hu et al. (2013). Fig. 6b shows the annual change rate of the diurnal $O_3$ concentration from 2006 to 2015 at XJH and PD sites respectively. The $O_3$ concentrations present increasing trends both in daytime (8:00-18:00, LST) and nighttime (19:00-07:00, LST) at XJH and PD sites, which is consistent with the results in Fig. 2. The nighttime $O_3$ concentrations increase more significantly than daytime $O_3$ at XJH, with the increasing rate of 1.239 and 0.956 ppbv $yr^{-1}$ respectively. While at PD site the $O_3$ concentrations increase by 1.338 ppbv $yr^{-1}$ in daytime which is higher than that in nighttime of 1.028 ppbv $yr^{-1}$. In comparison, the nighttime $O_3$ concentrations exhibit higher increasing rate at downtown site XJH than that at sub-urban site PD due to more NO emissions or more intensified urbanization (Hu et al., 2013). These results suggest that the reduction of $NO_x$ concentration from 2006 to 2015 has different effects on daytime and nighttime $O_3$ variations. The $O_3$ concentration in nighttime is more sensitive to $NO_x$ reduction at downtown, resulting in less $O_3$ lost compared with that in daytime. The results in Fig. 6b also show that the increasing rate of nighttime $O_3$ in downtown site XJH is higher than that at

sub-urban site PD due to the more reduction of $NO_x$ concentration in downtown area. Furthermore, the seasonal variability of daytime and nighttime $O_3$ concentrations at XJH site are illustrated in Fig. 7. Both daytime and night $O_3$ concentrations present increasing trends in all seasons. In comparison, the larger increasing rates of nighttime $O_3$ concentration are observed in spring, summer and autumn than that in daytime. For example, the nighttime $O_3$ concentrations increase at 1.341, 1.159 and 1.525 ppbv $yr^{-1}$ in spring, summer and autumn respectively, which are more significant than that of 1.008, 0.378 and 1.370 ppbv $yr^{-1}$ in daytime. The variability of winter $O_3$ concentrations in daytime and nighttime are generally close perhaps due to the lower $O_3$ photochemical productions. Hu et al. (2016) suggested that the nighttime boundary layer tended to be less stable resulted from the enhanced sensible heat flux in urban area, thus leading to more active nighttime turbulence. The sounding measurements at 20:00 (LST) in Shanghai are used to calculate the vertical temperature gradient between 1000 hPa and 925 hPa to indicate the intensity of nighttime turbulence, while presenting no significant trend from 2010 to 2015. Furthermore the PBL height retrieved from Lidar measurements at 20:00 (LST) presents the similar results as soundings. Based on the above measurements, the variation of turbulence at night may have only minor contribution to the nighttime $O_3$ increasing in Shanghai. However the effect of dry deposition could not be excluded by lacking of measurements, which need further investigation.

**Figure 6.** (a) The mean diurnal variation of $O_3$ concentration (ppbv) compared between 2006 and 2015 in XJH (red dots) and PD (blue dots). (b) The annual change rate of diurnal $O_3$ concentration (ppbv.$yr^{-1}$) from 2006 to 2015 at downtown site XJH (red bars) and sub-urban site PD (blue bars).

**Figure 7.** The daytime (8:00-18:00, LST) and nighttime (19:00-07:00, LST) $O_3$ variability from 2006 to 2015 at downtown site XJH in (a) spring, (b) summer, (c) autumn and (d) winter.

## 4 WRF-Chem study on the $O_3$ variation response to emission change

### 4.1 Design of the model experiments scheme

To better understand the role of $NO_x$ emission reduction in $O_3$ variation, the WRF-Chem model is utilized to calculate the changes of $O_3$ concentrations. Lin et al. (2017) suggested that the $NO_x$ emission was reduced in Shanghai in recent years resulted from the implementation of the Shanghai Clean Air Action Plan. The $NO_x$ emission in 2015 is estimated at $33.4\times10^4$ ton in Shanghai, reduced significantly by 30% compared with that in 2009 of $44.9\times10^4$ ton. Thus it provided the good opportunity to examine the $O_3$ variation response to the reduction of $NO_x$ emission in Shanghai. The $NO_x$ emissions in 2009 and 2015 are put into WRF-Chem model respectively to calculate the $O_3$ concentration. The other emissions (including gas and particulate matter) and meteorology used in WRF-Chem are set to be same. As a result, the difference of $O_3$ concentrations calculated by WRF-Chem is solely attributed to the change of $NO_x$ emission between 2009 and 2015, which is furthermore compared with the measurements.

The MIRAGE-shanghai field campaign was conducted in September of 2009 to explore the $O_3$ chemical formation and transformation in Shanghai (Tie et al., 2013). The mean temperature, mean wind speed and total precipitation in this month is 25 $^oC$, 2.85 m $s^{-1}$ and 89.5 mm respectively, which is very close to the climatological conditions during the past ten years from

2006 to 2015, with 24.7 $^{o}$C for mean temperature, 2.81 m $s^{-1}$ for mean wind speed, and 126 mm for total precipitation respectively. In addition, Shanghai is located at the typical sub-tropical area. The meteorology in September is characterized as the low cloud cover and rain occurrence, the slight wind speed and humidity, as well as the moderate solar radiation intensity. As suggested by Tie et al. (2013), the chemical age of $O_3$ plume in Shanghai urban area in September of 2009 was very young, indicating that the $O_3$ production was more dependent on the local emissions under such kind of meteorology, hence providing more insights into the $O_3$ chemical mechanism response to the local emission changes. We chose the meteorology in September of 2009 as the atmospheric background for all the sensitive experiments by WRF-Chem.

Tie et al. (2009a; 2013) highlighted that the WRF-Chem model was capable of studying the chemical and physical processed of $O_3$ in September of 2009 during the MIRAGE-Shanghai campaign. The calculated $O_3$, $NO_x$, VOCs and aerosols by WRF-Chem in clean and polluted episodes were fairly in agreement with the measurements except HONO, suggesting that the emission inventory in 2009 used in the model is reasonable for the Shanghai region. Moreover the VOCs emission in Shanghai is greatly improved according to the measurements from the MIRAGE-shanghai field campaign by Tie et al. (2013). Such emission from Tie et al. (2013) representing 2009 scenario is used in this study to conduct the control experiment (T1) as the baseline to simulate the $O_3$ and $NO_x$ concentrations in September of 2009. The T1 experiment is composed of 30 model runs for each day in September of 2009. Each model run is initiated at the 20:00 (LST) and performed for 52 h integrations. The first 28 h integration is regarded as model spin-up periods, the results from the later 24 h integration is captured hourly and averaged for mean daily concentration of $O_3$ and $NO_x$. The aim of the T1 experiment is to further evaluate the reliability of the emission inventory in 2009 used in WRF-Chem by fully comparing the calculated $O_3$ and $NO_x$ concentrations with in-situ measurements of 6 sites over Shanghai.

### 4.2 The NOx emission in 2009 used for base experiment

The distribution of $NO_x$ emission of 2009 scenario (Tie et al., 2013) in Shanghai used in WRF-Chem model has been showed in Fig. 1b. The $NO_x$ emission is mostly distributed in the urban zones, suggesting that transportation is the important source. The $NO_x$ is largely exported in downtown and two neighboring sub-urban zones in the east and north respectively. The maximum $NO_x$ emission is estimated at 16 kg $hr^{-1}$ $km^{-2}$ at downtown, compared with 2-6 kg $hr^{-1}$ $km^{-2}$ in the sub-urban area. In addition, there is a small town located in the south of Shanghai with the similar intensity of $NO_x$ emission as the sub-urban zones. The total $NO_x$ emission of 2009 scenario in Shanghai (Fig. 1b) is estimated at $41.4\times10^4$ ton in the model, which is close to the $47.8\times10^4$ ton suggested by Lin et al. (2017) according to the Shanghai Environmental Year Book.

### 4.3 Performance evaluation on the base experiment

The mean daytime and nighttime $O_3$ concentrations in September 2009 are calculated by WRF-Chem and compared with measurements over 6 sites in Shanghai, which are presented in Fig. 8a and b respectively. Both modeled and measured $O_3$ concentrations in daytime are higher than that in nighttime. The calculated daytime $O_3$ concentration is about 10-18 ppbv higher than that in nighttime in urban region, which is consistent with the measured difference of 12-14 ppbv at XJH and PD sites. The observed daytime and nighttime $O_3$ concentrations at remote site DT show the minimum difference of 5 ppbv which is also captured by WRF-Chem model due to the

less impact of anthropogenic emissions. In Fig. 8a, there exists a large $O_3$ plume with high concentration of 40-48 ppbv in daytime in the west of Shanghai and its neighboring area from WRF-Chem simulations. It is also illustrated by the daytime $O_3$ measurements at SS site with 40 ppbv. However such daytime $O_3$ plume dissipates at night (Fig. 8b) leading to the significant difference of $O_3$ concentration between day and night. Tie et al. (2013) suggested the enhancement of $O_3$ concentration in the downwind of Shanghai due to the considerable $O_3$ formation in the aged city plume transported westerly in September resulted from the dominant east winds. According to the study of Tie et al. (2013), the $O_3$ concentrations had a minimum within 20 km of the city, and enhanced at the west of 100–150 km away from the city in daytime, which was consistent with the results in Fig. 8a. In addition, both model simulations and in-situ measurements in daytime and nighttime highlight the lower $O_3$ concentration in urban zones than that in suburb. The simulated daytime and nighttime $O_3$ concentration in downtown is 28-32 ppbv and 12-14 ppbv respectively, significantly lower than that at sub-urban (36-38 ppbv and 26-28 ppbv respectively) and rural area (40-42 ppbv and 36-38 ppbv respectively). Similarly, the measured daytime $O_3$ concentration at downtown site XJH is 28 ppbv, lower than that at sub-urban site PD and remote site DT by 12 ppbv and 21 ppbv respectively. Geng et al. (2007) suggested that under VOC-limited regime, the lower $O_3$ concentration in downtown was resulted from the higher $NO_x$ emission, which depressed the $O_3$ production process. Under high $NO_x$ conditions, the OH radicals are lost by the reaction of $\mathrm{NO_2 + OH \rightarrow HNO_3}$ (Sillman, 1995). As a result, higher $NO_x$ concentration in urban area leads to lower OH concentration, which results in smaller $O_3$ production. Tang et al. (2008) also suggested that the $O_3$ concentration in Shanghai downtown was higher on weekends than that on weekdays due to the reduced $NO_x$ concentration. However the discrepancy is also evident between model results and measurements. For example, the modeled nighttime $O_3$ concentrations at XJH and PD are about 2-6 ppbv lower than the measurements, perhaps due to the uncertainty of $NO_x$ emission in urban area suggested by Tie et al. (2009a). In addition, the calculated daytime $O_3$ concentrations in the remote site DT and chemical site JS are lower than measurements by 10 ppbv and 6 ppbv respectively. The former is resulted from the overestimation of the wind speed by WRF-Chem model leading to excessive $O_3$ transport for underestimation (Zhou et al., 2017). While the latter is mainly due to the prominent underestimation of the VOCs emission in the chemical zones suggested by Tie et al. (2009a).

**Figure 8.** The calculated distribution of (a) daytime and (b) nighttime $O_3$ concentration by WRF-Chem (shade) in September of 2009 compared with measurements (circles) of 6 sites over Shanghai. The minimum $O_3$ concentrations in daytime and nighttime both occur in urban center.

Fig. 9a and b show the daily variations of $O_3$ and $NO_x$ concentrations compared between WRF-Chem simulations and the in-situ measurements over 5 sites. The statistical analysis of model performance for $O_3$ and $NO_x$ is listed in Table 1 and Table 2 respectively. The calculated magnitude and daily variation of $O_3$ concentrations agree well with the measurements, suggesting that both meteorology and photochemistry are well reproduced by WRF-Chem model. For example, the Root Mean Square Error (RMSE) calculated between modeled and measured $O_3$ concentration are 7.4, 10.5, 12, 8.6, 9.2 ppbv for XJH, JS, DT, PD and BS respectively, and the difference between the simulation results and in-situ measurement is below 10%, which are very

satisfactory compare with the similar works by Geng et al (2007) and Tie et al. (2013). The correlated coefficients (R) for the mean daily $O_3$ concentration range from 0.6 to 0.8 above 99% confidence over 5 sites, indicating good consistency of day by day variations between the model results and measurements. Comparably the $O_3$ concentration is best simulated by WRF-Chem at the downtown site XJH and sub-urban site PD with the lower RMSE and better R. However the discrepancy of daily $O_3$ concentration between the model and measurements is also evident. For example, a rapid change of $O_3$ concentration from 16 to 19 in September was observed over all sites, indicating it's a regional event instead of a local phenomenon. The $O_3$ concentration firstly increases significantly during 16-19 (episode-1), then sharply decreased during the later 4 days (episode-2). The similar rapid $O_3$ change in Shanghai was also reported by Tie et al. (2009a), and their explanation is that this episode was mainly related to the intensity of the sub-tropical high-pressure system on Pacific Ocean in summer. The model captures the $O_3$ variations and magnitudes during the both risen and fallen episodes very well at downtown site XJH, but substantially underestimates the increasing variability of $O_3$ concentration during episode-1 at sub-urban and rural sites by 10-15 ppbv. Geng et al. (2008a) suggested the "chemical transport of $O_3$" from Shanghai downtown area to the distance of 18-36 km far away, which increased the $O_3$ concentration at sub-urban or rural sites. This "chemical transport of $O_3$" is difficult to be reflected by WRF-Chem model due to the current inventory is too coarse to accurately reflect the detailed distribution and variation of $NO_x$ emission, e.g. the $NO_x$ emission from mobile source in the city. In addition, the underestimation of the $O_3$ concentration at suburb of Shanghai in summer is possibly attributed to the model bias of sea breeze simulations. Under the condition of weak sub-tropical pressure, the sea breeze develops at noontime to yield a cycling wind pattern in Shanghai, leading to the rapid accumulation of high $O_3$ concentration. The WRF-Chem usually underestimates the sea surface temperature, which tends to accelerate the sea breeze development and weak the $O_3$ trapping in the city (Tie et al., 2009a). The calculated daily $NO_x$ concentration by WRF-Chem compared with measurements are shown in Fig. 9b. Both the modeled and measured $NO_x$ concentrations at the remote site DT are very low, with the average of 1.4 and 2.9 ppbv respectively due to seldom anthropogenic emissions there. The calculated $NO_x$ concentration at XJH and PD are generally well consistent with the measurements with the excellent R of 0.8 and 0.82 and small RMSE of 6.9 and 7.5 ppbv respectively. However the $NO_x$ concentration is underestimated by WRF-Chem at sub-urban site BS in the steel zone. The calculated $NO_x$ concentration at BS is 16.1 ppbv, which is lower than the measurements by 5 ppbv. The difference of $NO_x$ concentrations between the model and observations is generally above 10%, suggesting the performance of $NO_x$ simulation is somewhat lower than that of $O_3$. It was also reported by Tie et al. (2007; 2009b; 2013), during the evaluation of the $NO_x$ calculations by WRF-Chem in MIRAGE-Shanghai and MIRAGE-mex campaign studies. The lifetime of $NO_x$ at the surface is about 1-2 days, shorter than $O_3$. Thus the $NO_x$ concentration is determined by the detailed emissions and dynamical factors, which need to develop the advanced inventory with higher resolution to reproduce both the spatial distributions and temporal variations of $NO_x$ emission.

**Figure 9.** The calculated mean daily concentrations (ppbv) of (a) $O_3$ and (b) $NO_x$ at 5 sites in September of 2009 by WRF-Chem (red circles) and compared with measurements (blue circles).

### 4.4 Sensitive study on the $O_3$ variability response to the emission change

The T1 experiment shows the excellent performance for $O_3$ and $NO_x$ simulations, including the spatial distribution pattern, and the day by day variation and magnitude. It is indicated that the emission in 2009 scenario used in WRF-Chem is reasonable, and the model is efficient for conducting the sensitive studies on $O_3$ variation response to the emission change. In order to better understand the measured long-term trend of $O_3$ concentration during the past ten years in Shanghai and its relationship to the emission reduction, several sensitive studies are conducted in this study (Table 3). The control study of T1 is conducted based on the $NO_x$ emission in 2009 scenario in Shanghai. According to the study of Lin et al. (2017), the $NO_x$ emission in 2015 in Shanghai is reduced by 30% compared with that in 2009. Thus we conduct the sensitive experiment T2 by WRF-Chem, cutting the $NO_x$ emission by 30% compared with T1, whereas keeping the other emissions and meteorology same as T1. As a result, the calculated $O_3$ difference between T1 and T2 is likely attributed to the $NO_x$ emission reduction between 2015 and 2009.

Fig. 10a shows the distribution of the difference of $O_3$ concentration simulated by T1 and T2 (T2-T1). The reduction of $NO_x$ emission has the obvious effect on the magnitude and distribution of $O_3$ concentration. The $O_3$ concentration increases notably in urban area corresponding to the higher $NO_x$ emissions in Fig. 1, ranging from 2-7 ppbv. The enhancement of $O_3$ concentration is most significant in downtown and neighboring sub-urban zones, as well as the southern town, generally more than 4 ppbv. For example, the maximum increase in $O_3$ concentration is 6.4 ppbv occurred at downtown site XJH, followed by 4-5 ppbv at sub-urban site PD. The increasing rates of $O_3$ trend at XJH and PD are estimated at 1.06 ppbv $yr^{-1}$ and 0.96 ppbv $yr^{-1}$ from 2009 to 2015 by WRF-Chem, which is consistent to the observed $O_3$ growth variability of 1-1.3 ppbv $yr^{-1}$. The response of $O_3$ concentration to the $NO_x$ reduction is not evident in the rural area including the eastern part of Shanghai and the island with low $NO_x$ emissions. The comparison of T1 and T2 further illustrates the speculation that the significant increasing trend of $O_3$ concentration during the past ten years in Shanghai is mostly attributed to the reduction of $NO_x$ emission as a result of the implementation of Shanghai Clean Air Action Plan.

The $O_3$ chemical formation is strongly related to $NO_x$ and VOCs concentrations. As discussed by Geng et al. (2008a) the $O_3$ chemical formation is clearly under VOC-limited regime in Shanghai and its neighboring area. Under the high $NO_x$ condition, NO tends to react with $O_3$ instead of $NO_2$, flowing by $NO_2 + OH \rightarrow HNO_3$, causing the decrease of the reactivity and ensuing $O_3$ concentrations. Thus reduced $NO_x$ emission would result in increase in $O_3$ concentration, which has been discussed in Fig. 10a.

Despite of minor change of VOCs in the last ten years, it is worth to investigate the effect of the VOCs changes on $O_3$ concentrations in Shanghai. For this purpose, we conduct a sensitive study (T3), with 50% increase of VOCs emission compared with T1, but keeping $NO_x$ and other emissions as well as the meteorology same as T1. For RADM2 gas mechanism used in WRF-Chem, the VOCs are surrogated into 14 species, such as alkane, alkene, aromatic, formaldehyde, etc. All the species of VOCs are increased by 50% at every model grid over Shanghai and at every hour. The difference of $O_3$ concentration between T3 and T1 (T3-T1) is shown in Fig. 10b. As we expected, the $O_3$ concentration in Shanghai is sensitive to the enhancement of VOCs emission, increased by 3-4 ppbv in urban area due to more NO is converted to $NO_2$ by reaction with $RO_2$ and $HO_2$. Furthermore, the abundant $O_3$ plumes produced in the urban zones significantly

transport to the downwind areas about 100-200 km away, resulting in elevated $O_3$ concentration in the western Shanghai by about 2 ppbv. According to Tie et al. (2013), the $O_3$ plume released in Shanghai urban area can be transported to downwind of the city by about 100-150 km away in the MIRAGE-shanghai field campaign. The model studies of T1, T2 and T3 highlight that under the emission of 2009 scenario, the $O_3$ chemical production is clearly under VOC-limit regime, either decreasing $NO_x$ concentration or increasing VOCs concentration would result in the $O_3$ enhancement. The analysis on in-situ measurements and model experiments jointly suggests that the significant $O_3$ increasing trend during the past ten years in Shanghai is mainly attributed to the large reduction of $NO_x$ emission.

**Figure 10.** The difference of O3 concentration (ppbv) between (a) T2 and T1 (T2-T1), (b) T3 and T1 (T3-T1) respectively conducted by WRF-Chem model. The difference between T2 and T1 lies in the $NO_x$ emissions set in T2 (2015 scenario) is 30% lower than that in T1 (2009 scenario), which is estimated by Lin et al. (2017) according to the Shanghai Environment Yearbook. The difference between T3 and T1 is dependent on that the VOCs emission in T3 is 50% higher than that in T1.

### 4.5 The variation of $O_3$ production regime response to emission change

The $O_3$ chemical mechanism in Shanghai was explored by several studies based on the in-situ measurements around 2008 and 2009. Geng et al. (2008a; 2008b), Ran et al. (2009) and Tie et al. (2009a) all revealed that the $O_3$ production around 2008 and 2009 in Shanghai was clearly under VOC-limit regime which was further illustrated by the above model studies. As indicated in Fig. 3, the significant decrease of $NO_x$ concentration is observed from 2009 to 2015 in Shanghai, while the VOCs concentration changed little during the same period. As we know, the $O_3$ chemical formation is strongly related to $NO_x$ and VOCs concentrations with nonlinearity. Thus the different variability of $NO_x$ and VOCs concentration from 2009 to 2015 inevitably has the large effect on the $O_3$ production regime, which need to be investigated deeply.

The complex relationship among $NO_x$, VOCs and $O_3$ concentrations is usually depicted by $O_3$ isopleths diagram. The $O_3$ isopleths plot (Fig. 11) in Shanghai used in this study is constructed by the OZIPR model based on the in-situ measurements of $O_3$, $NO_x$, VOCs and meteorology. Under high VOCs and low $NO_x$ condition (low $NO_x$/VOCs ratio), the $O_3$ production is not sensitive to VOCs, while positively correlated to $NO_x$ concentration, which is viewed as $NO_x$-limited regime. By contrast, under low VOCs and high $NO_x$ condition (high $NO_x$/VOCs ratio), the $O_3$ production tends to increase with the VOCs growth or $NO_x$ reduction, which is regarded as VOC-limited regime. The $NO_x$-limited and VOC-limited regime is divided by a ridge line (the dot-dash line in Fig. 11) in the $O_3$ isopleths plot. The $O_3$ production is not sensitive to either $NO_x$ concentration or VOCs concentration when near the ridge line, which is regarded as the transition regime.

The $O_3$ chemical production regime at XJH and PD in 2009 and 2015 is positioned respectively in Fig. 11. In 2009 the $O_3$ production at both XJH and PD sites (marked as red and blue hollow circle respectively) are clearly under VOC-limited regime. Thus decrease in $NO_x$ concentration leads to the $O_3$ enhancement, which is highlighted by the previous in-situ measurements and model experiments. Since then the $O_3$ production regime tends to move toward the dot-dash line due to the significant reduction of $NO_x$ concentration accompanied with the relative less change of VOCs at the two sites. In 2015 the $O_3$ production at XJH (marked as red

solid circle) is still under VOC-limited regime, but for PD (marked as blue solid circle), it is close to the dot-dash line, approaching the transition regime between VOC-limited to $NO_x$-limited. This result suggests that if the $NO_x$ emission keeps reduction after 2015 assuming the VOCs concentration keeps constant, the $O_3$ concentration will continue to increase at XJH, while at PD the $O_3$ concentration is supposed to be insensitive to the $NO_x$ change. According to the $O_3$ chemical regime depicted in Fig. 11, if the $NO_x$ concentration decreases by 5 ppbv after 2015, the peak $O_3$ concentration at XJH will further increase by 3 ppbv, whereas at PD it seems to change very slightly. To better understand this further change, more sensitive studies of WRF-Chem are conducted in the following sections.

**Figure 11.** The $O_3$ chemical production at downtown site XJH and sub-urban site PD in 2009 and 2015 depicted by $O_3$ isopleths diagram. The hollow and solid red circles denote $O_3$ production regime at XJH in 2005 and 2019 respectively. The hollow and solid blue circles denote $O_3$ production regime at PD in 2005 and 2019 respectively.

## 5 The future $O_3$ evaluation

### 5.1 The $O_3$ level in 2020

According to the Shanghai Clean Air Action Plan, the $NO_x$ emission in Shanghai will be further reduced by 20% in 2020 compared with that in 2015. According to the above analysis based on the $O_3$ isopleths plot (Fig. 11), the $O_3$ concentrations in downtown and sub-urban seem to have distinct different responses to further $NO_x$ reduction after 2015. In order to better understand the future $O_3$ variation, the sensitive experiment T4 is conducted by WRF-Chem with 20% reduction of $NO_x$ emission compared with T2. The $NO_x$ emissions set in T2 and T4 represent 2015 and 2020 scenario respectively. The other emissions and meteorology are set to be same as T1. The difference of $O_3$ concentration between T2 and T4 (T4-T2) is presented in Fig. 12a. The $O_3$ concentration keeps increasing in downtown area such as XJH site, ranging from 2-4 ppbv. However, for the sub-urban zones such as the PD site, the $O_3$ concentration changes very little response to the further $NO_x$ reduction, ranging from 0-1 ppbv. As discussed in Fig. 11, in 2015 the $O_3$ production at PD is possibly under the transition regime from VOC-limited to $NO_x$-limited near the ridge line. As a result, the $O_3$ concentration is not sensitive to the variation of $NO_x$ concentration. However the $O_3$ concentration in the rural zones generally decreases by 1ppbv, indicating that with the further $NO_x$ reduction after 2015 the $O_3$ chemical production transfers from VOCs-limited to $NO_x$-limited regime in the rural of Shanghai.

It is suggested in Fig.11 that the $O_3$ production at downtown site XJH in 2015 is still under VOC-limited regime despite of the significant $NO_x$ reduction. The $O_3$ concentration would be also sensitive to the variation of VOCs concentration. Thus the sensitive experiment T5 is conducted by WRF-Chem model with 50% enhancement of VOCs emission compared with T2 (representing the emission in 2015 scenario). It is presented in Fig. 12b that the $O_3$ concentration increases by 2-3 ppbv in downtown area due to the enhancement of VOCs, suggesting that the $O_3$ production at downtown in 2015 is still under VOC-limited regime, which is consistent with the results in Fig. 11. Moreover the $O_3$ plumes produced in urban area transport to the downwind area to accumulate the high $O_3$ concentration in the western area to Shanghai by 2 ppbv. While at sub-urban site PD, the $O_3$ concentration changes less than 1 ppbv response to the increase in

VOCs emission, which is similar as the very weak $O_3$ variations relative to the $NO_x$ reduction in Fig. 12a. Overall, the models studies of T4 and T5 jointly suggest that the $O_3$ concentration at sub-urban site PD in 2015 is not sensitive to either $NO_x$ or VOCs variations due to the $O_3$ production is under the transition regime depicted in the $O_3$ isopleths plot.

**Figure 12.** The difference of $O_3$ concentration (ppbv) between (a) T4 and T2 (T4-T2), (b) T5 and T2 (T5-T2) respectively conducted by WRF-Chem model. The difference between T4 and T2 is that the $NO_x$ emissions set in T4 (2020 scenario) is 20% lower than that in T2 (2015 scenario), which is estimated according to the Shanghai Clean Air Action Plan. The difference between T5 and T2 lies in that the VOCs emission in T5 is 50% higher than that in T2.

### 5.2 The $O_3$ chemical production after 2020

The above study shows that the $O_3$ production at sub-urban site PD in 2020 will likely transfer from VOCs-limited regime to $NO_x$-limited regime without consideration of possible VOCs changes. For the purpose to better understand the $O_3$ pollution control strategy, it is worth to estimate the $O_3$ level response to emission change after 2020 in Shanghai. It is also essential to access how many $NO_x$ emission need to be cut after 2020 will cease the $O_3$ enhancement in downtown area. Thus the sensitive experiment T6 is conducted by further 20% reduction of $NO_x$ emission from 2020 scenario (T4). The difference of $O_3$ concentration between T6 and T4 (T6-T4) is shown in Fig. 13a. It is clear that the $O_3$ concentration at downtown keeps nearly constant regardless of the further reduction of $NO_x$ emission after 2020. That is to say the increasing trend of $O_3$ in downtown with the $NO_x$ reduction ceases after 2020, indicating that the $O_3$ production likely approachs the transition regime. In addition, the $O_3$ concentration decreases significantly out of the downtown area, ranging from 2-3 ppbv in sub-urban zones, and more than 4 ppbv in rural, indicating that the $O_3$ production in Shanghai transfers to $NO_x$-limited regime after 2020 except the downtown area where the $O_3$ production is likely near the transition zone. On the other hand, if the $NO_x$ emission is kept constant after 2020 as T4, while the VOCs emission is increased by 50% from T4 (T7 experiment), the $O_3$ concentration (Fig. 13b) changes little in both urban and suburb area in Shanghai which is different from the previous model study of T5 the T3 when $O_3$ production is under VOC-limited condition. It is suggested that the $O_3$ concentration after 2020 is not sensitive to the variation of VOCs concentration because the continuous reduction of $NO_x$ emission keeps in promoting the $O_3$ production to transfer into $NO_x$-limited regime. Thus further reduction of $NO_x$ tends to decrease the $O_3$ concentration in Shanghai.

**Figure 13.** The difference of O3 concentration (ppbv) between (a) T6 and T4 (T6-T4), (b) T7 and T4 (T7-T4) respectively conducted by WRF-Chem model. The $NO_x$ emissions set in T6 is 20% lower than that in T4 (2020 scenario). The VOCs emission in T7 is 50% higher than that in T4.

## Conclusions

$O_3$ pollution is a serious issue in China. Better understanding the elevated $O_3$ and its response to emission change is important for Chinese megacities. In this study, we analyze the increasing trend of $O_3$ concentration by long-term measurements of $O_3$ and its precursors as well as meteorology in Shanghai combined with the WRF-Chem model. The $O_3$ production regime

response to the emission change in Shanghai during the past ten years is also explored by $O_3$ isopleths plot. In addition, the future $O_3$ variation and its chemical production in Shanghai are evaluated by WRF-Chem model. The main conclusions are summarized as follows:

(1) The daily maximum $O_3$ concentration measured in Shanghai increased significantly from 2006 to 2015 with the rate of 0.808 ppbv $yr^{-1}$ at downtown site XJH and 1.374 ppbv $yr^{-1}$ at sub-urban site PD respectively. The observed increasing trend of $O_3$ is not limited in the urban zones but expanded to the larger scale covering the total Shanghai city. The $NO_x$ and VOCs concentrations presented different variability from $O_3$ during the same period, in which $NO_x$ concentration decreases significantly at both XJH and PD sites, whereas the VOCs changes very little without evident trend.

(2) Because there are minor trends of measured $O_3$ photolysis, local dispersion and regional transport resulted from meteorology, it is speculated that the significant $O_3$ increasing trend during 2006 to 2015 in Shanghai is likely attributed to the reduction of $NO_x$ concentration as a result of the strong VOCs-limited regime for $O_3$ production. The nighttime $O_3$ is more sensitive to $NO_x$ reduction than that in daytime at downtown, because less $O_3$ is depressed by NO in nighttime. As a result, the observed nighttime $O_3$ concentration at XJH increases more rapidly than that in daytime response to the $NO_x$ reduction.

(3) The WRF-Chem model is utilized to calculate the long term $O_3$ variations response to emission change. The sensitive experiments illustrate that either reduction of $NO_x$ emission or growth of VOCs emission conducted by WRF-Chem lead to the significant enhancement in $O_3$ concentration in urban zones in 2009 as the baseline, indicating the $O_3$ production is clearly under VOC-limited regime. The calculated $O_3$ concentration increases by 1-7 ppbv in urban zones from 2009 to 2015 resulted from 30% reduction of $NO_x$ emission estimated by Shanghai Environmental Monitoring Center. The enhancement of $O_3$ concentration is significant in urban zones generally more than 4 ppbv, with the maximum elevation of 6-7 ppbv occurred at downtown area, which is consistent with the measurements. The increasing rates of $O_3$ trend at downtown site XJH and sub-urban site PD are estimated at 1.06 ppbv $yr^{-1}$ and 0.96 ppbv $y^{r-1}$ from 2009 to 2015 by WRF-Chem, which is close to the observed $O_3$ growth variability of 1-1.3 ppbv $yr^{-1}$. This result suggests that the observed increasing trend of $O_3$ concentration during the past ten years in Shanghai is likely attributed to the reduction of $NO_x$ emission under the VOC-limited condition for $O_3$ production.

(4) The model sensitive study suggests that significant decrease in $NO_x$ concentration combined with the obscure VOCs variation from 2006 to 2015 gradually promotes the $O_3$ chemical production in Shanghai from VOC-limited to $NO_x$-limited, which is consistent with the $O_3$ isopleths diagram. The $O_3$ isopleths plot shows that $O_3$ production is in VOC-limited regime in both downtown site XJH and sub-urban site PD in 2009. With the 30% reduction of $NO_x$ emission from 2009 to 2015 estimated by Shanghai Environmental Monitoring Center, the $O_3$ production in XJH is still under VOC-limited regime, while the $O_3$ production moves to the transition regime in PD, suggesting that the $O_3$ concentration in sub-urban zones is not sensitive to the variation of either $NO_x$ or VOCs concentration.

(5) In order to better understand the $O_3$ control strategy in Shanghai, the future $O_3$ production is estimated by WRF-Chem. The $O_3$ concentration in Shanghai downtown would keep increasing till 2020 with the 20% reduction of $NO_x$ emission after 2015 estimated by Shanghai Clean Air Action Plan. If the $NO_x$ emission is further decreased by 20% after 2020, The $O_3$

concentration will decrease by 2-3 ppbv in sub-urban zones, and more than 4 ppbv in suburb. While the $O_3$ concentration in downtown is not sensitive to either $NO_x$ reduction or VOCs enhancement after 2020, indicating the $O_3$ production in shanghai will transfer to $NO_x$-limited regimes except downtown where the $O_3$ production is likely close to the transition regime. Further reduction of $NO_x$ emission after 2020 tend to mitigate the $O_3$ pollution in Shanghai.

(6) There are some uncertainties and limitations existed in the study. First, the inhomogeneity of the $NO_x$ reduction is not considered in the sensitive experiments by lacking of the high resolution emission inventory (e.g. 1 km resolution). Second, the variation of VOCs emission is not taken into account in the model experiments due to the more uncertainties existed in the current VOCs emission inventory. While $O_3$ production in Shanghai is very sensitive to some VOC species, especially aromatics. Thus the accurate emission inventory of VOCs need to be developed and included in the future study. Third, the same meteorology is used for all WRF-Chem simulations. However the $O_3$ photolysis, advection, and vertical diffusion are all strongly affected by meteorology. The change of meteorology would be considered and evaluated in the future studies for more deep investigation.

***Data availability***. The data used in this paper can be provided upon request from Jianming Xu (metxujm@163.com).

***Author contributions***. XT came up with the original idea of investigating the impact of emission change on long term O3 variations by. XT and JX designed the analysis method. JX conducted the analysis. WG, YL and QF provided the observational data and helped in discussion.

***Competing interests***. The authors declare that they have no conflict of interest.

***Acknowledgements.*** This study was funded by the National Key R&D Program of China (grant 2018YFC0213800), the National Natural Science Foundation of China (91644223, 41430424, 41730108 and 41801367).

**References**


Binkowski, F. S. and Roselle, S. J.: Models-3 community multi scale air quality (CMAQ) model aerosol component – 1. Model description, Journal of Geophysical Research, 108 (D6), 4183, doi:10.1029/2001jd001409, 2003.

Brasseur, G. P., Orlando, J. J., and Tyndall, G. S.: Atmospheric chemistry and global change, Oxford University Press, Cambridge, USA, 654 pp., 1999.

Cai, C. J., Geng, F. H., Tie, X. X., Yu, Q., and An J. L.: Characteristics and source apportionment of VOCs measured in Shanghai, China, Atmospheric Environment, 44, 5005-5014, 2010.

Chen, F. and Dudhia, J.: Coupling an advanced land surface hydrology model with the Penn State-NCAR MM5 modeling system, Part I: Model implementation and sensitivity, Monthly Weather Review, 129, 569–585, 2001.

Dudhia, J.: Numerical study of convection observed during the winter monsoon experiment using a mesoscale two-dimensional model, Journal of the Atmospheric Sciences, 46, 3077–3107, 1989.

Emmons, L. K., Walters, S., Hess, P. G., Lamarque, J. F., Pfister, G. G., Fillmore, D., Granier, C., Aguenther, A., Kinnison, D., Laepple, T., Orlando, J., Tie, X., Tyndall, G., Wiedinmyer, C., Baughcum, S. L., and Kloster, S.: Description and evaluation of the model for ozone and related chemical tracers, version4 (MOZART-4), Geoscientific Model Development, 3, 43–67, 2010.

Gao, W., Tie, X. X., Xu, J. M., Huang, R. J., Mao, X. Q., Zhou, G. Q., and Chang, L. Y.: Long-term trend of $O_3$ in a mega City (Shanghai), China: Characteristics, causes, and interactions with precursors, Science of the Total Environment, 603-604, 425-433, 2017.

Geng, F. H., Zhao, C. S., Tang, X., Lu, G. L., and Tie, X. X.: Analysis of ozone and VOCs measured in Shanghai: a case study, Atmospheric Environment, 41, 989–1001, 2007.

Geng, F. H., Tie, X., Xu, J., Zhou, G., Peng, L., Gao, W., Tang, X., Zhao, C.: Characterizations of ozone, $NO_x$, and VOCs measured in Shanghai, China, Atmospheric Environment, 42, 6873–6883, 2008a.

Geng, F. H., Zhang, Q., Tie, X., Huang, M., Ma, X., Deng, Z., Quan, J., and Zhao, C.: Aircraft measurements of $O_3$, $NO_x$, CO, VOCs, and $SO_2$ in the Yangtze River Delta region, Atmospheric Environment, 43, 584–593, 2008b.

Geng, F. H., Tie, X., Guenther, A., Li, G., Cao, J., and Harley, P.: Effect of isoprene emissions from major forests on ozone formation in the city of Shanghai, China, Atmospheric Chemistry and Physics, 11, 10449–10459, 2011.

Geng, F. H., Mao, X. Q., Zhou, M. Y., Zhong, S. Y., and Lenschow, D.: Multi-year ozone concentration and its spectra in Shanghai, China, Science of the Total Environment, 521-522, 135-143, 2015.

Gery, M. W., and Crouse, R. R.: User's Guide for Executing OZIPR, Atmospheric Research and Exposure Assessment Lab., Office of Research and Development, U.S. EPA, Research Triangle Park, N. C., http://www.epa.gov/scram001/models/other/oziprdme.txt, 2002.

Grell, G. A., Peckham, S. E., Schmitz, R., McKeen, S. A., Frost, G., Skamarock, W. C., and Eder, B.: Fully coupled "online" chemistry within the WRF model, Atmospheric Environment, 39, 6957–6975,2005.

Guenther, A., Karl, T., Harley, P., Wiedinmyer, C., Palmer, P. I., and Geron, C.: Estimates of global terrestrial isoprene emissions using MEGAN (Model of Emissions of Gases and Aerosols from

Nature), Atmospheric Chemistry and Physics, 6, 3181–3210, 2006.
Hong, S. Y. and Lim, J. O. J.: The WRF Single-Moment 6-Class Microphysics Scheme (WSM6), Journal of the Korean Meteorological Society, 42, 129–151, 2006.
Hu, X. M., Klein, P. M., and Xue, M.: Evaluation of the updated YSU planetary boundary layer scheme within WRF for wind resource and air quality assessments, Journal of Geophysical Research-Atmospheres, 118, 10490-10505, 2013.
Hu, X. M., Xue, M., Klein, P. M., Illston, B. G., and Chen, S.: Analysis of Urban Effects in Oklahoma City using a Dense Surface Observing Network, Journal of Applied Meteorology and Climatology, 55, 723-741, 2016.
Lei, W., Foy, B. de, Zavala, M., Volkamer, R., and Molina, L. T.: Characterizing ozone production in the Mexico City Metropolitan Area: a case study using a chemical transport model, Atmospheric Chemistry and Physics, 7, 1347-1366, 2007.
Li, G., Lei, W., Zavala, M., Volkamer, R., Dusanter, S., Stevens, P., and Molina, L. T.: Impacts of HONO sources on the photochemistry in Mexico City during the MCMA-2006/MILAGO Campaign, Atmospheric Chemistry and Physics, 10, 6551–6567, 2010.
Li, G., Bei, N., Tie, X., and Molina, L. T.: Aerosol effects on the photochemistry in Mexico City during MCMA-2006/MILAGRO campaign, Atmospheric Chemistry and Physics, 11, 5169–5182, 2011.
Li, K., Jacob, D. J., Liao, H., Shen, L., Zhang, Q., and Bates, K. H.: Anthropogenic drivers of 2013-2017 trends in summer surface ozone in China, PANS, 116, 2, 422-427, 2019.
Lin, X., Trainer, M., and Liu, S. C.: On the nonlinearity of the tropospheric ozone production, Journal of Geophysical Research Atmospheres, 93 (D12), 15879–15888, 1988.
Lin, Y. F., Wang, Q., Fu, Q. Y., Duan, Y. S., Xu, J. M., Liu, Q. Z., Li, F., and Huang, K.: Temporal-spatial characteristics and impact factors of ozone pollution in Shanghai, Environmental Monitoring in China (in Chinese), 33, 4, 60-67, 2017.
Lin, Y. L., Farley, R. D., and Orville, H. D.: Bulk parameterization of the snowfield in a cloud model, Journal of Climate and Applied Meteorology, 22, 1065–1092, 1983.
Lu, X., Hong, J., Zhang, L., Cooper, O., Schultz, M., Xu, X., Wang, T., Gao, M., Zhao, Y., and Zhang, Y.: Severe surface ozone pollution in China: A global perspective, Environmental Science &Technology Letters, 5, 487–494, 2018.
Monks, P. S., Archibald, A. T., Colette, A., Cooper, O., Coyle, M., Derwent, R., Fowler, D., Granier, C., Law, K. S., Mills, G. E., Stevenson, D. S., Tarasova, O., Thouret, V., von Schneidemesser, E., Sommariva, R., Wild, O., and Williams, M. L.: Tropospheric ozone and its precursors from the urban to the global scale from air quality to short-lived climate forcer, Atmospheric Chemistry and Physics, 15, 8889–8973, 2015.
Ma, Z., Xu, J., Quan, W., Zhang, Z., Lin, W., and Xu, X.: Significant increase of surface ozone at a rural site, north of eastern China, Atmospheric Chemistry and Physics, 16, 3969–3977, 2016.
Nenes, A., Pandis, S. N., and Pilinis, C.: ISORROPIA: A new thermodynamic equilibrium model for multiphase multicomponent inorganic aerosols, Aquatic Geochemistry, 4, 123–152, 1998.
Ran, L., Zhao, C., Geng, F., Tie, X., Tang, X., Peng, L., Zhou, G., Yu, Q., Xu, J., and Guenther, A.: Ozone photochemical production in urban Shanghai, China: analysis based on ground level observations, Journal of Geophysical Research Atmospheres, 114, D15301, 2009.
Sillman, S.: The use of NOy, H2O2, and HNO3 as indicators for ozone-NOx-hydrocarbon sensitivity in urban locations, Journal of Geophysical Research Atmospheres, 100, 14175–14188, 1995.

Sillman, S.: The relation between ozone, $NO_x$ and hydrocarbons in urban and polluted rural environments, Atmospheric Environment, 33, 1821–1845, 1999.

Song, J., Lei, W., Bai, N., Zavala, M., de Foy, B., Volkamer, R., Cardenas, B., Zheng, J., Zhang, R., and Molina L. T.: Ozone response to emission changes: a modeling study during the MCMA-2006/MILAGRO Campaign, Atmospheric Chemistry and Physics, 10, 3827-3846, 2010

Stockwell, W. R., Middleton, P., Chang, J. S., and Tang, X.: The second generation regional acid deposition model chemical mechanism for regional air quality modeling, Journal of Geophysical Research Atmospheres, 95, 16343–16367, 1990.

Sun, L., Xue, L., Wang, T., Gao, J., Ding, A., Copper, O., Lin, M., Xu, P., Wang, Z., Wang, X., Wen, L., Zhu, Y., Chen, T., Yang, L., Wang, Y., Chen, J., and Wang, W.: Significant increase of summertime ozone at Mount Tai in central eastern China, Atmospheric Chemistry and Physics, 16, 10637–10650, 2016.

Tai, A. P. K., Martin, M. V., and Heald, C. L.: Threat to future global food security from climate change and ozone air pollution, Nature Climate Chang, 4, 817–821, 2014.

Tang, G., Li, X., Wang, Y., Xin, J., and Ren, X.: Surface ozone trend details and interpretations in Beijing, 2001–2006, Atmospheric Chemistry and Physics, 9, 8813–8823, 2009.

Tang, W. Y., Zhao, C. S., Geng, F. H., Peng, L., Zhou, G. Q., Gao, W., Xu, J. M., and Tie, X. X.: Study of ozone "weekend effect" in Shanghai, Science in China Series D: Earth Sciences, 51, 9, 1354-1360, 2008.

Tie, X., Brasseur, G., Emmons, L., Horowitz, I., and Kinnison, D.: Effects of aerosols on tropospheric oxidants: a global model study, Journal of Geophysical Research Atmospheres, 106, 22931–22964, 2001.

Tie, X., Madronich, S., Walters, S., Zhang, R. Y., Rasch, P., and Collins, W.: Effect of clouds on photolysis and oxidants in the troposphere, Journal of Geophysical Research Atmospheres, 108, 4642, doi:10.1029/2003jd003659, 2003.

Tie, X., Madronich, S., Li, G., Ying, Z., Zhang, R., Garcia, A., Taylor, J., and Liu, Y.: Characterizations of chemical oxidants in Mexico City: A regional chemical dynamical model (WRF-Chem) study, Atmospheric Environment, 41, 1989-2008, 2007.

Tie, X., Geng, F. H., Peng, L., Gao, W., Zhao, C. S.: Measurement and modeling of $O_3$ variability in Shanghai, China: application of the WRF-Chem model, Atmospheric Environment, 43, 4289–4302, 2009a.

Tie, X., Madronich, S., Li, G., Ying, Z., Weinheimer, A., Apel, E., and Campos, T.: Simulation of Mexico City plumes during the MIRAGE-Mex field campaign using the WRF-Chem model, Atmospheric Chemistry and Physics, 9, 4621-4638, 2009b.

Tie, X., Geng, F., Guenther, A., Cao, J., Greenberg, J., Zhang, R., Apel, E., Li, G., Weinheimer, A., Chen, J., and Cai, C.: Megacity impacts on regional ozone formation: observations and WRF-Chem modeling for the MIRAGE-Shanghai field campaign, Atmospheric Chemistry and Physics, 13, 5655–5669, doi:10.5194/acp-13-5655-2013, 2013.

Wang, H. J., and Chen, H. P.: Understanding the recent trend of haze pollution in eastern China: roles of climate change, Atmospheric Chemistry and Physics, 16, 4205–4211, 2016

Wang, T., Xue, L., Brimblecombe, P., Lam Y. F., Li, L., and Zhang, L.: Ozone pollution in China: A review of concentrations, meteorological influences, chemical precursors, and effects, Science of Total Environment, 575, 1582-1596, 2017.

Wesely, M. L.: Parameterization of surface resistances to gaseous dry deposition in regional-scale

numerical models, Atmospheric Environment, 23, 1293–1304, 1989.
Xu, J. M., Yan, F. X., Xie, Y., Wang, F. Y., Wu, J. B., and Fu, Q. Y.: Impact of meteorological conditions on a nine-day particulate matter pollution event observed in December 2013, Shanghai, China, Particuology, 20, 69–79, 2015.
Xu, J. M., Chang, L. Y., Yan, F. X., and He, J. H.: Role of climate anomalies on decadal variation in the occurrence of wintertime haze in the Yangtze River Delta, China, Science of the Total Environment, 599-600, 918-925, 2017.
Ying, Z. M., Tie, X., and Li, G. H.: Sensitivity of ozone concentrations to diurnal variations of surface emissions in Mexico City: A WRF/Chem modeling study, Atmospheric Environment, 43, 851–859, 2009.
Zhang, Q., Streets, D. G., Carmichael, G. R., He, K. B., Huo, H., Kannari, A., Klimont, Z., Park, I. S., Reddy, S., Fu, J. S., Chen, D., Duan, L., Lei, Y., Wang, L. T., Yao, Z. L.: Asian emissions in 2006 for the NASA INTEX-B mission, Atmospheric Chemistry and Physics, 9, 5131-5153, 2009.
Zhao, S., Li, J. P., Sun, C.: Decadal variability in the occurrence of wintertime haze in central eastern China tied to the Pacific decadal oscillation, Scientific Reports, 6, 27424, 2016.
Zheng, B., Tong, D., Li, M., Liu, F., Hong, C., Geng, G., Li, H., Li, X., Peng, L., Qi, J., Yan, L., Zhang, Y., Zhao, H., Zheng, Y., He, K., and Zhang, Q.: Trends in China's anthropogenic emissions since 2010 as the consequence of clean air actions, Atmospheric Chemistry and Physics, 18, 14095-14111, https://doi.org/10.5194/acp-18-14095-2018, 2018.
Zhou, G. Q., Xu, J. M., Xie, Y., Chang, L. Y., and Gao, W.: Numerical air quality forecasting over eastern China: An operational application of WRF-Chem, Atmospheric Environment, 153, 94-108, 2017.

**Table 1.** Statistical analysis on $O_3$ simulation in September of 2009 by WRF-Chem model compared with measurements of 5 sites (XJH, JS, DT, PD, BS) over Shanghai. MO and MM represent the mean value (unit: ppbv) of observed and modeled $O_3$ concentration respectively. RMSE and R are the Root Mean Square Error and correlated coefficient respectively calculated between modeled and measured $O_3$ concentration.

| | MO | MM | RMSE | R (99% confidence) |
|---|---|---|---|---|
| | | ppbv | | \ |
| **XJH** | 21.6 | 23.0 | 7.2 | 0.78 |
| **JS** | 34.6 | 30.0 | 10.3 | 0.64 |
| **DT** | 47.3 | 40.3 | 12.0 | 0.61 |
| **PD** | 33.5 | 34.9 | 8.6 | 0.74 |
| **BS** | 31.7 | 31.2 | 9.3 | 0.67 |

**Table 2.** Statistical analysis on $NO_x$ simulation in September of 2009 by WRF-Chem model compared with measurements of 5 sites (XJH, JS, DT, PD, BS) over Shanghai. MO and MM represent the mean value (unit: ppbv) of observed and modeled $NO_x$ concentration respectively. RMSE and R are the Root Mean Square Error and correlated coefficient respectively calculated between modeled and measured $NO_x$ concentration.

| | MO | MM | RMSE | R (99% confidence) |
|---|---|---|---|---|
| | | ppbv | | \ |
| **XJH** | 32.1 | 33.7 | 7.0 | 0.74 |
| **JS** | 14.9 | 14.7 | 7.6 | 0.61 |
| **DT** | 3.0 | 1.5 | 2.3 | 0.6 |
| **PD** | 20.3 | 16.8 | 7.5 | 0.82 |
| **BS** | 21.6 | 16.1 | 9.8 | 0.8 |

**Table 3.** Scheme of WRF-Chem sensitivity simulations.

| Simulation | $NO_x$ EI | VOCs EI | Meteorology |
|---|---|---|---|
| **T1 (Control Run)** | 2009 | 2009 | September of 2009 |
| **T2** | 2015 (30% reduction) | 2009 | September of 2009 |
| **T3** | 2009 | 50% increasing | September of 2009 |
| **T4** | 2020 (50% reduction) | 2009 | September of 2009 |
| **T5** | 2015 | 50% increasing | September of 2009 |
| **T6** | 70% reduction | 2009 | September of 2009 |
| **T7** | 2020 (50% reduction) | 50% increasing | September of 2009 |

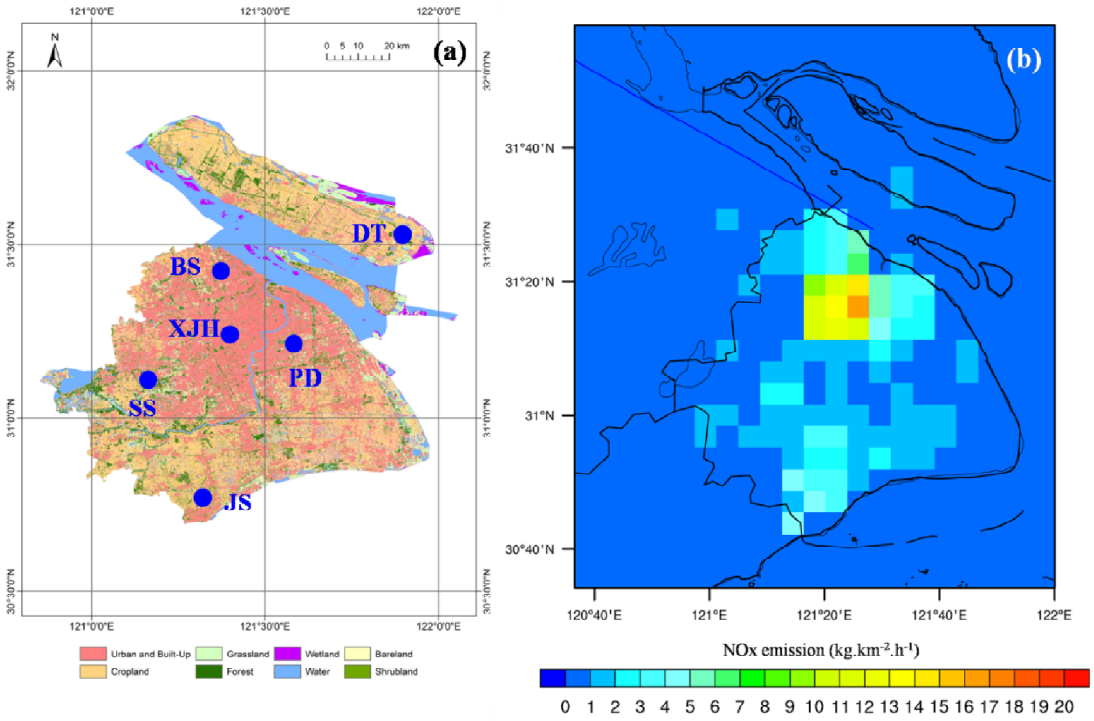


**Figure1** (a) The distribution of land-use category in Shanghai. The blue dots denote the locations of 6 sties (XJH, BS, PD, SS, JS, DT). (b) The NOx emission of 2009 scenario in Shanghai.

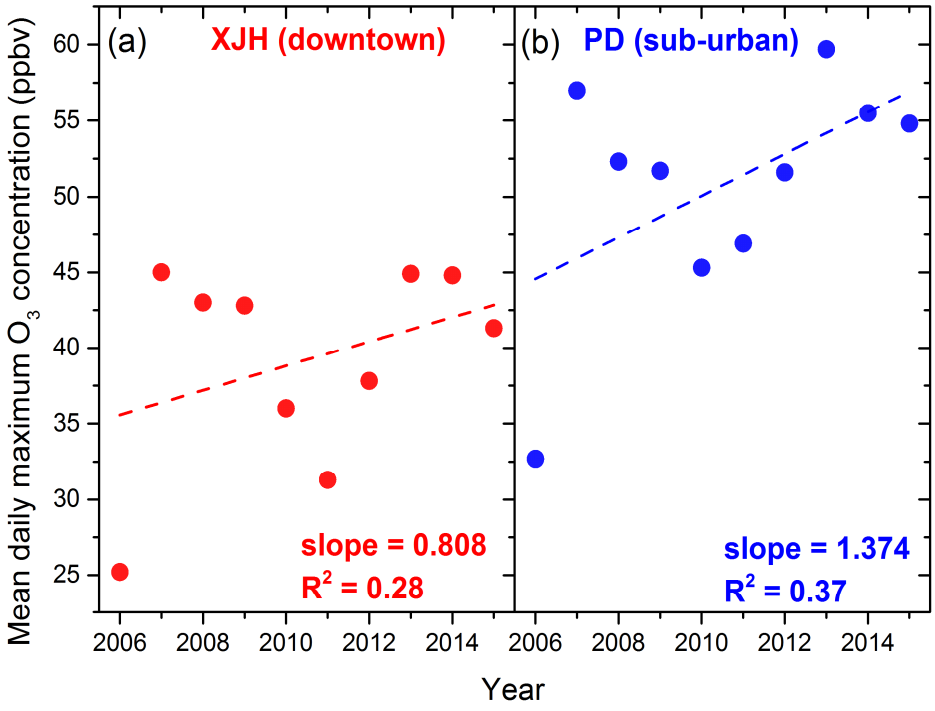


957

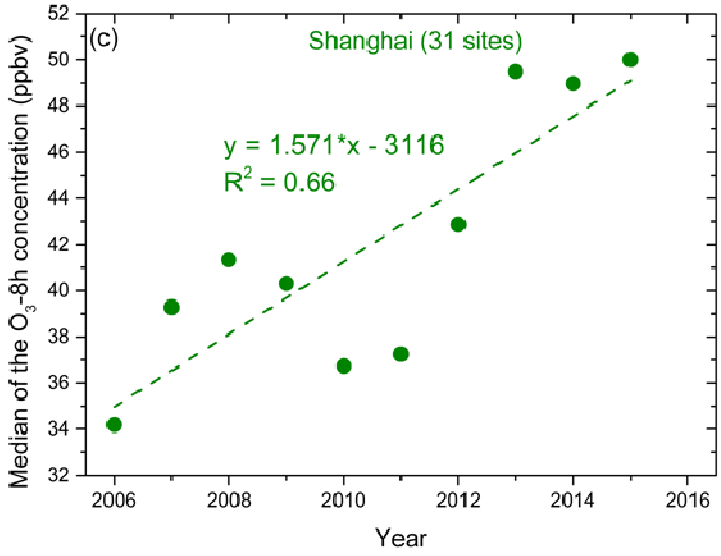


958

959 **Figure 2.** The annual variation of daily maximum $O_3$ concentration (ppbv) from 2006 to 2015 at (a)
960 downtown site XJH and (b) sub-urban site PD, both presenting the significant increasing trends
961 with 0.808 ppbv $yr^{-1}$ at XJH and 1.374 ppbv $yr^{-1}$ at PD respectively. The variation of the median
962 8-h $O_3$ concentration (ppbv) from 2006 to 2015 averaged for 31 sites over Shanghai (c), also
963 shows the increasing variability of 1.571 ppbv $yr^{-1}$.

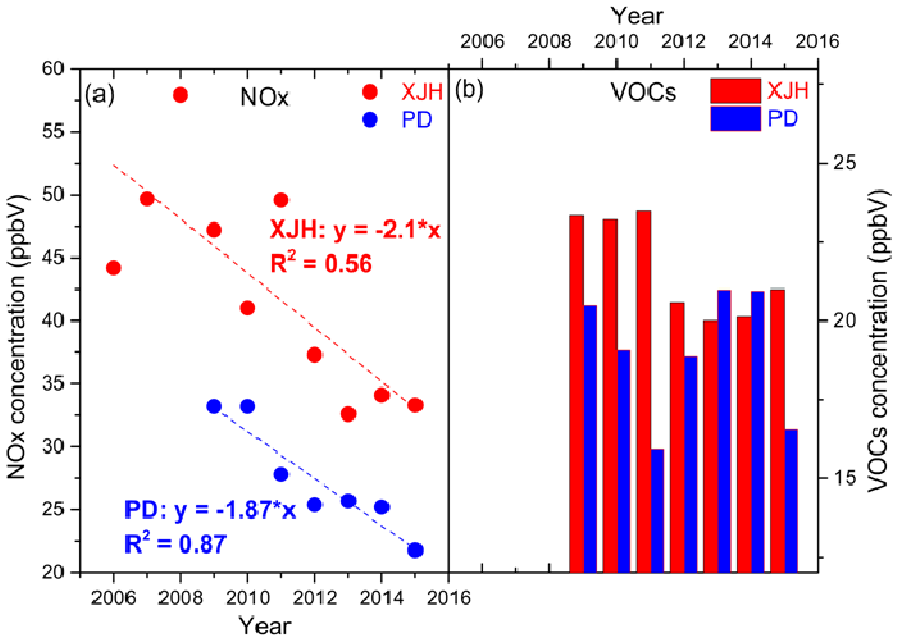


964

965 **Figure 3.** The mean annual concentrations (ppbv) of (a) $NO_x$ (dots) and (b) VOCs (bars) from 2006
966 to 2015 at downtown site XJH and sub-urban site PD respectively. The $NO_x$ concentrations at XJH
967 and PD both present obvious decreasing trends with 2.1 ppbv $yr^{-1}$ and 1.87 ppbv $yr^{-1}$. While the
968 VOCs concentrations at both sites present no clear inter-annual trends.

969

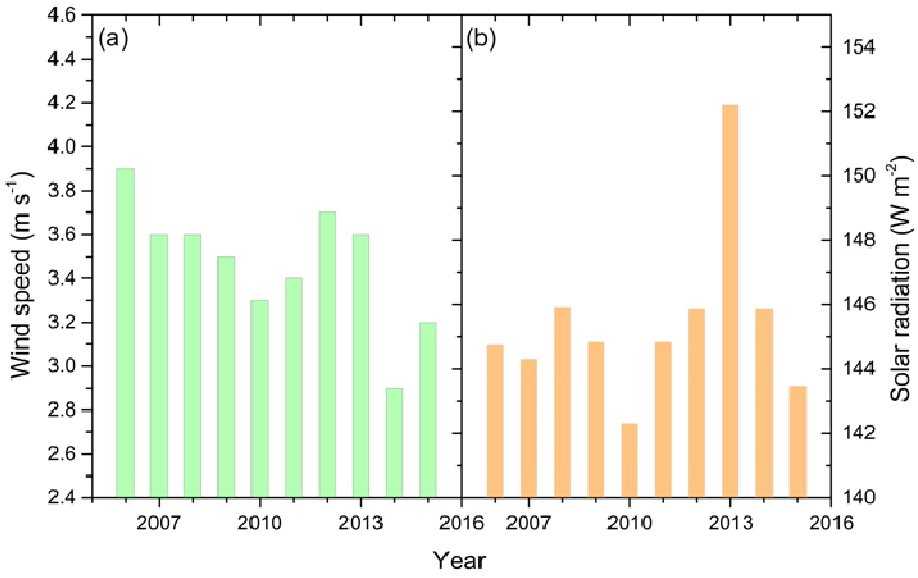


970

971 **Figure 4.** The annual variation of (a) summer wind speed (m $s^{-1}$) and (b) total solar radiation (W
972 $m^{-2}$) from 2006 to 2015 in Shanghai. Both wind speed and the solar radiation present weak
973 inter-annual variations but without significant trends.

974

975

976

977

978

979

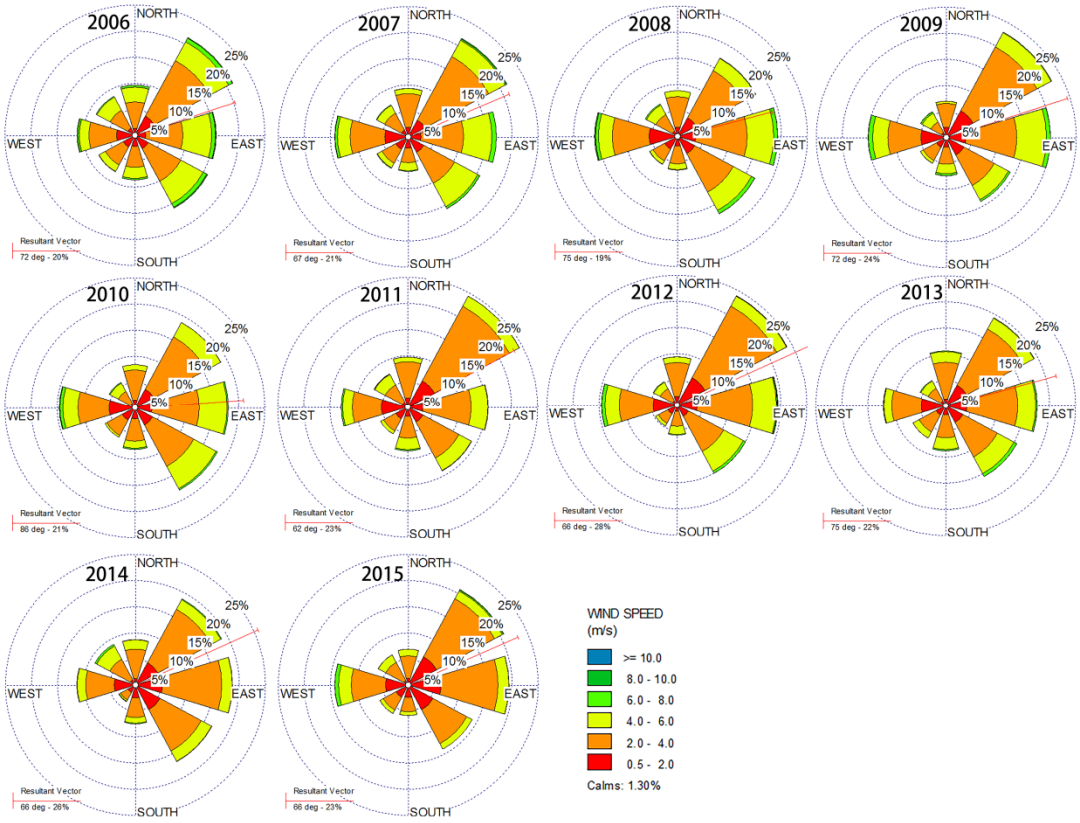


980

981 **Figure 5.** The wind rose of each year from 2006 to 2015 in Shanghai. The red line means the
982 resultant vector suggesting the dominant wind direction.

983

984

985

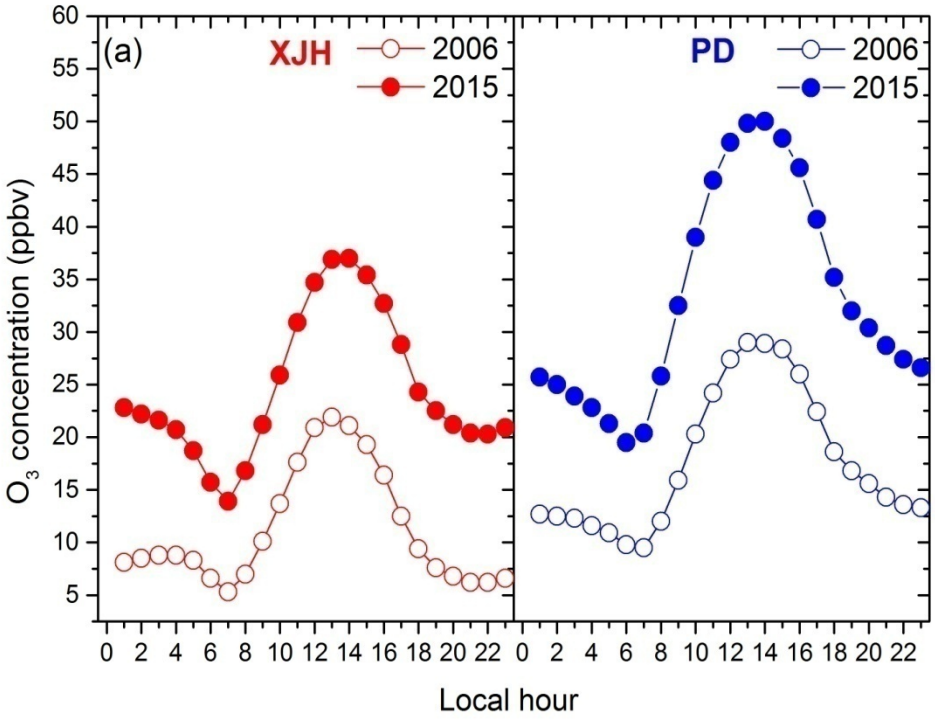


986

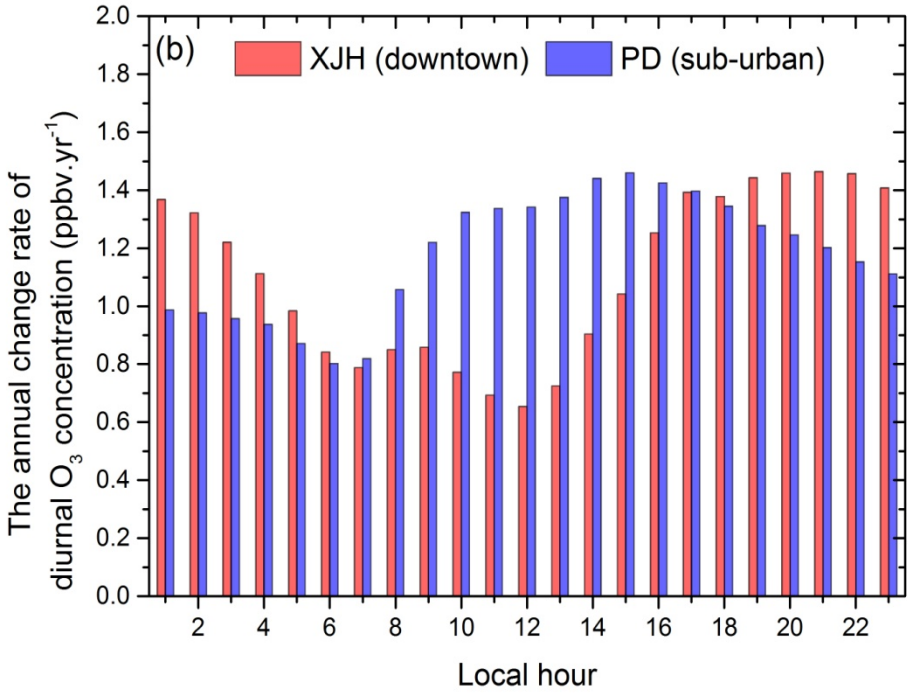


**Figure 6.** (a) The mean diurnal variation of $O_3$ concentration (ppbv) compared between 2006 and 2015 in XJH (red dots) and PD (blue dots). (b) The annual change rate of diurnal $O_3$ concentration (ppbv.yr$^{-1}$) from 2006 to 2015 at downtown site XJH (red bars) and sub-urban site PD (blue bars).

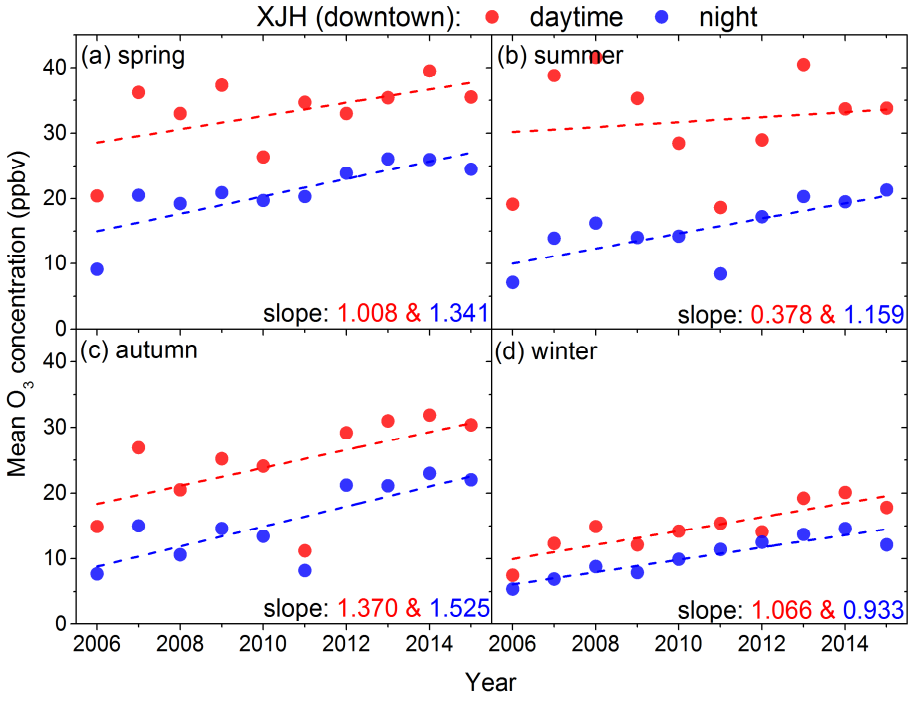


**Figure 7.** The daytime (8:00-18:00, BJT) and nighttime (19:00-07:00, BJT) $O_3$ variability from 2006 to 2015 at downtown site XJH in (a) spring, (b) summer, (c) autumn and (d) winter.

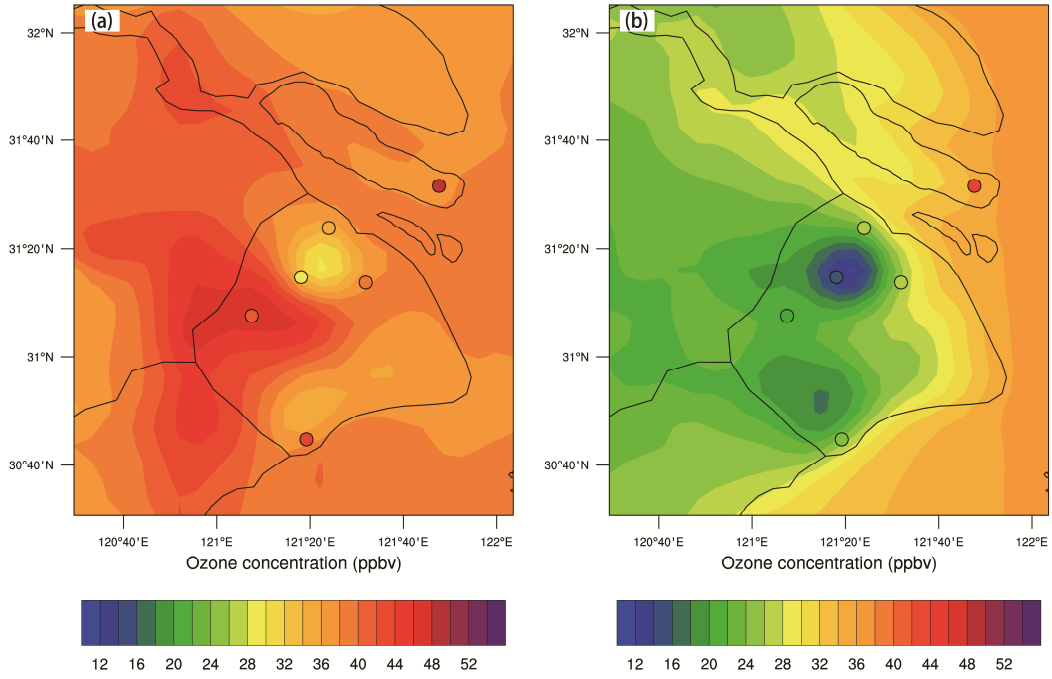


997

998 **Figure 8.** The calculated distribution of (a) daytime and (b) nighttime $O_3$ concentration by
999 WRF-Chem (shade) in September of 2009 compared with measurements (circles) of 6 sites over
1000 Shanghai. The minimum $O_3$ concentrations in daytime and nighttime both occur in urban center.
1001

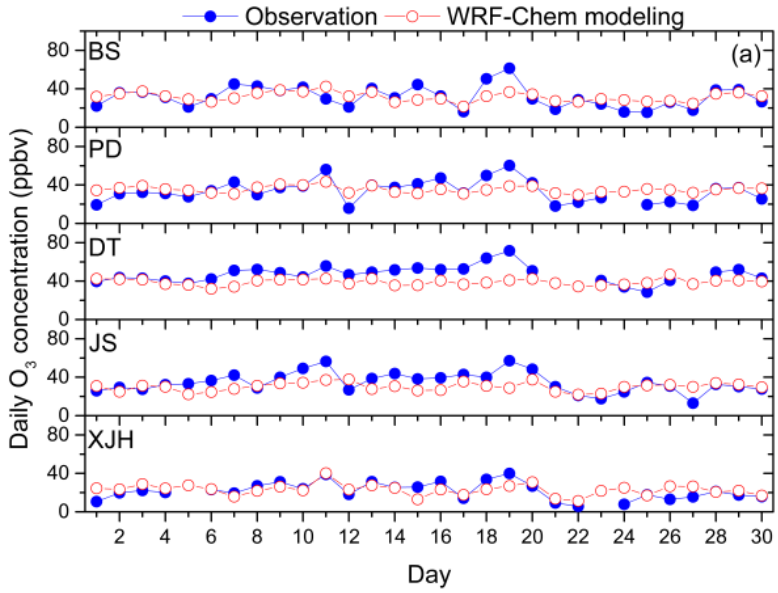


1002

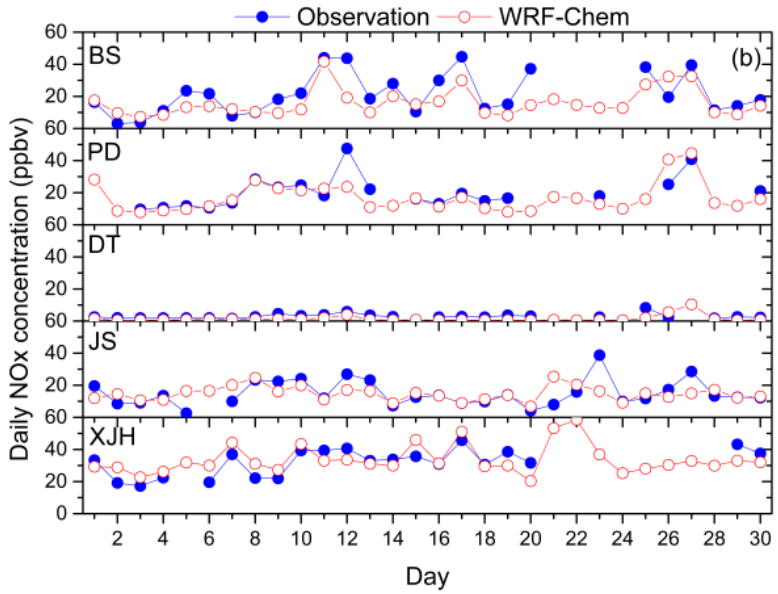


1003

1004 **Figure 9.** The calculated mean daily concentrations (ppbv) of (a) $O_3$ and (b) $NO_x$ at 5 sites in
1005 September of 2009 by WRF-Chem (red circles) and compared with measurements (blue circles).
1006

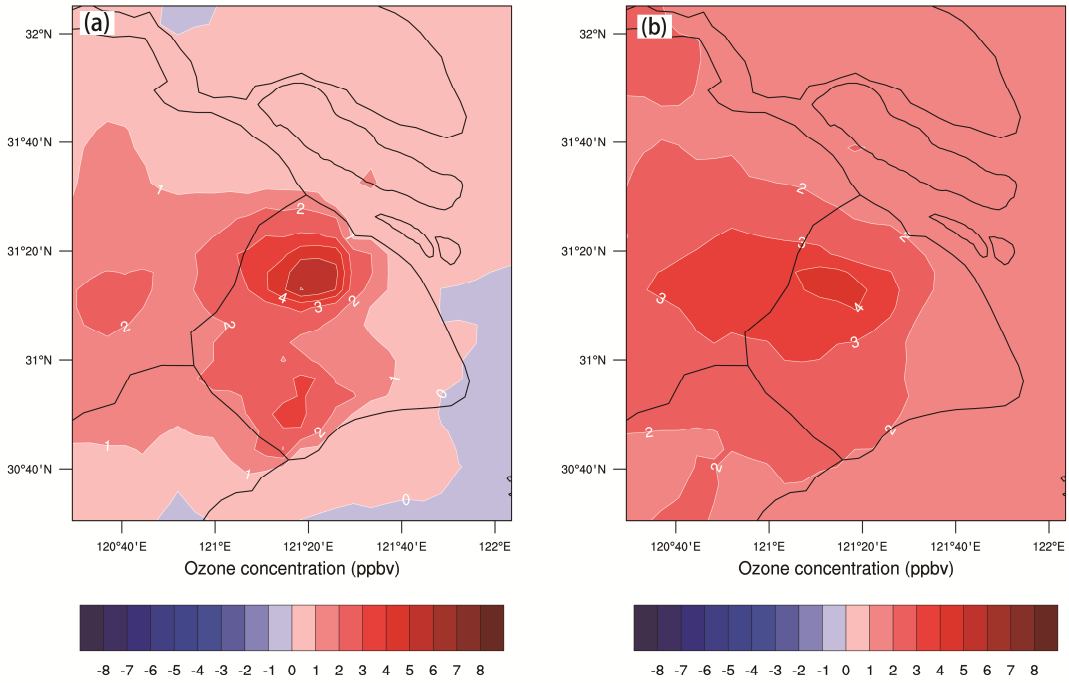


**Figure 10.** The difference of O3 concentration (ppbv) between (a) T2 and T1 (T2-T1), (b) T3 and T1 (T3-T1) respectively conducted by WRF-Chem model. The difference between T2 and T1 lies in the $NO_x$ emissions set in T2 (2015 scenario) is 30% lower than that in T1 (2009 scenario), which is estimated by Lin et al. (2017) according to the Shanghai Environment Yearbook. The difference between T3 and T1 is dependent on that the VOCs emission in T3 is 50% higher than that in T1.

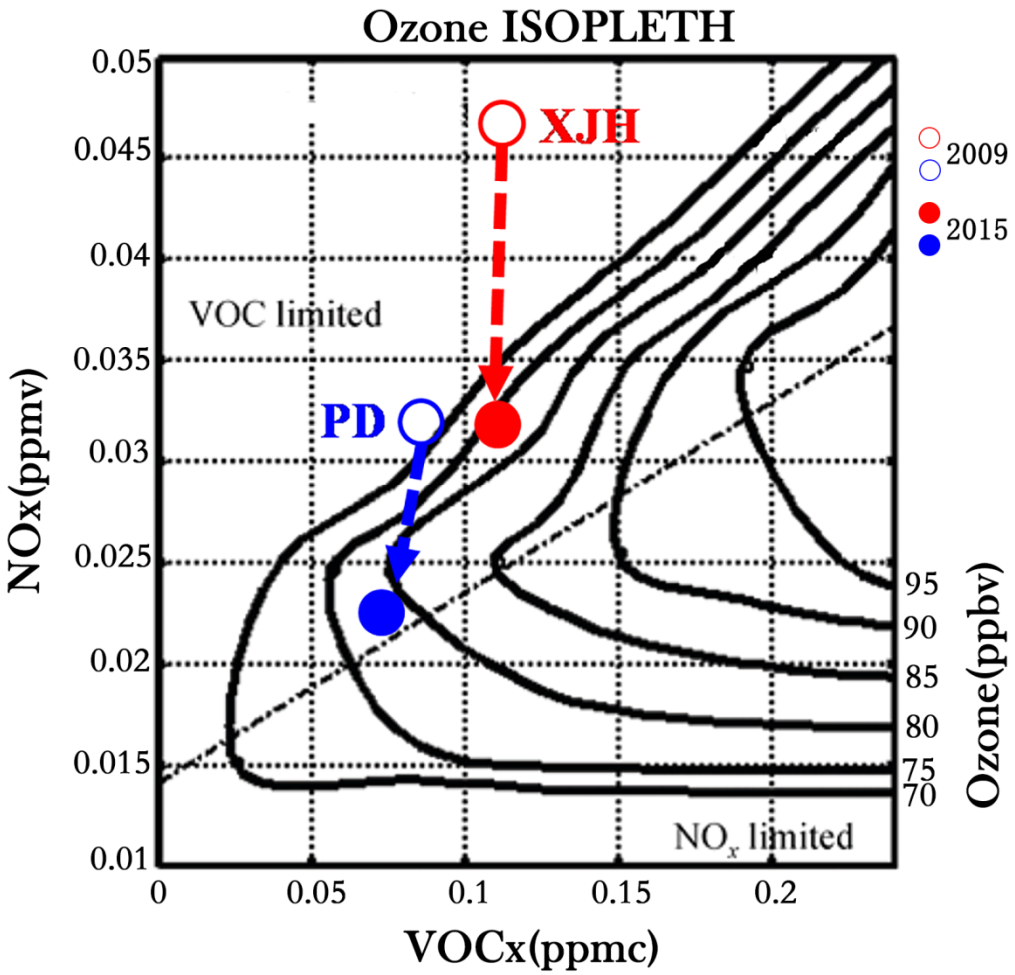


**Figure 11.** The $O_3$ chemical production at downtown site XJH and sub-urban site PD in 2009 and 2015 depicted by $O_3$ isopleths diagram. The hollow and solid red circles denote $O_3$ production regime at XJH in 2005 and 2019 respectively. The hollow and solid blue circles denote $O_3$ production regime at PD in 2005 and 2019 respectively

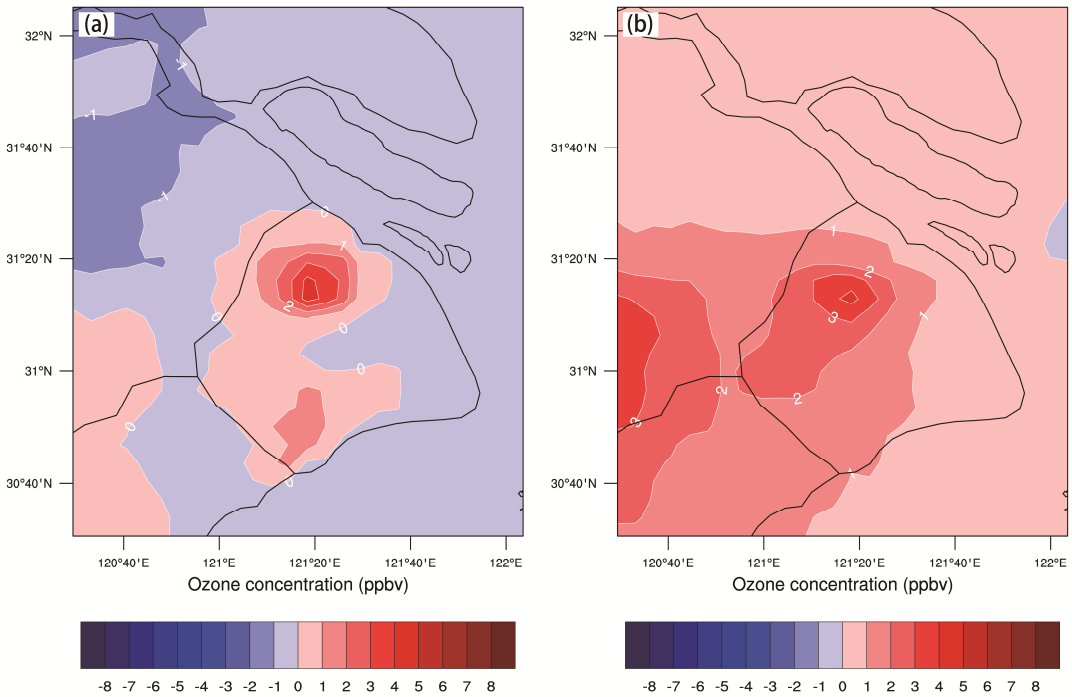


**Figure 12.** The difference of O3 concentration (ppbv) between (a) T4 and T2 (T4-T2), (b) T5 and T2 (T5-T2) respectively conducted by WRF-Chem model. The difference between T4 and T2 is that the $NO_x$ emissions set in T4 (2020 scenario) is 20% lower than that in T2 (2015 scenario), which is estimated according to the Shanghai Clean Air Action Plan. The difference between T5 and T2 lies in that the VOCs emission in T5 is 50% higher than that in T2.

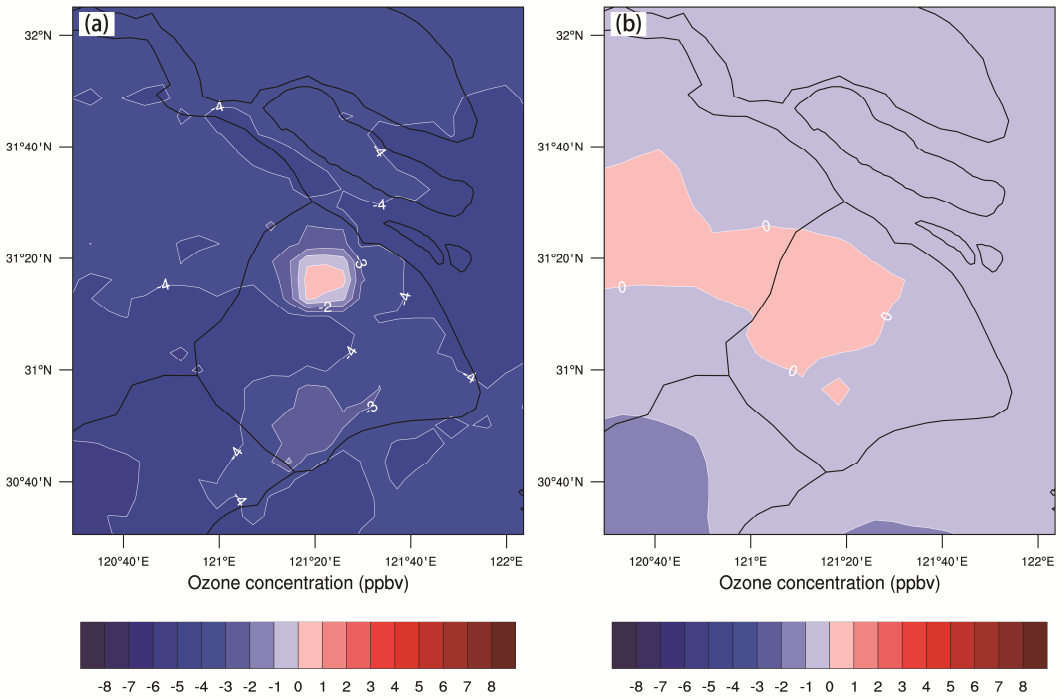


**Figure 13.** The difference of O3 concentration (ppbv) between (a) T6 and T4 (T6-T4), (b) T7 and T4 (T7-T4) respectively conducted by WRF-Chem model. The $NO_x$ emissions set in T6 is 20% lower than that in T4 (2020 scenario). The VOCs emission in T7 is 50% higher than that in T4.